Channel Shaping Using
Beyond Diagonal Reconfigurable Intelligent Surface: Analysis, Optimization, and Enhanced Flexibility

Yang Zhao, *Member, IEEE,* Hongyu Li, *Graduate Student Member, IEEE,*
Massimo Franceschetti, *Fellow, IEEE,* and Bruno Clerckx, *Fellow, IEEE*

Abstract—This paper investigates the capability of a passive Reconfigurable Intelligent Surface (RIS) to redistribute the singular values of point-to-point Multiple-Input Multiple-Output (MIMO) channels for achieving power and rate gains. We depart from the conventional Diagonal (D)-RIS with diagonal phase shift matrix and adopt a Beyond Diagonal (BD) architecture that offers greater wave manipulation flexibility through element-wise connections. Specifically, we first provide shaping insights by characterizing the channel singular value regions attainable by D-RIS and BD-RIS via a novel geodesic optimization. Analytical singular value bounds are then derived to explore their shaping limits in typical deployment scenarios. As a side product, we tackle BD-RIS-aided MIMO rate maximization problem by a local-optimal Alternating Optimization (AO) and a shaping-inspired low-complexity approach. Results show that compared to D-RIS, BD-RIS significantly improves the dynamic range of all channel singular values, the trade-off in manipulating them, and thus the channel power and achievable rate. Those observations become more pronounced when the number of RIS elements and MIMO dimensions increase. Of particular interest, BD-RIS is shown to activate multi-stream transmission at lower transmit power than D-RIS, hence achieving the asymptotic Degrees of Freedom (DoF) at low Signal-to-Noise Ratio (SNR) thanks to its higher flexibility of shaping the distribution of channel singular values.

Index Terms—Reconfigurable intelligent surface, channel singular value redistribution, rate maximization, manifold optimization.

I. INTRODUCTION

A. Background

Today we are witnessing a paradigm shift from connectivity to intelligence, where the wireless environment is no longer a chaotic medium but a conscious agent that can serve on demand. This is empowered by recent advances in Reconfigurable Intelligent Surface (RIS), a programmable passive planar surface that recycles and redistributes ambient electromagnetic waves for improved wireless performance. A typical RIS consists of numerous low-power sub-wavelength non-resonant scattering elements, whose response can be engineered in real-time to manipulate the amplitude, phase, frequency, and polarization of the scattered waves [1]. It enables low-noise full-duplex operation, featuring better flexibility than reflectarrays, lighter

Yang Zhao, Hongyu Li, and Bruno Clerckx are with the Department of Electrical and Electronic Engineering, Imperial College London, London SW7 2AZ, U.K. (e-mail: {yang.zhao18, c.li21, b.clerckx}@imperial.ac.uk).

Massimo Franceschetti is with the Department of Electrical and Computer Engineering, University of California, San Diego, La Jolla CA 92093, USA (e-mail: massimo@ece.ucsd.edu).

footprint than relays, and greater scalability than Multiple-Input Multiple-Output (MIMO) systems. One popular RIS research direction is *joint passive and active beamforming* design with transceivers to enhance a specific performance measure, which has attracted significant interests in wireless communication [2]–[4], sensing [5]–[7], and power transfer literature [8]–[10]. While passive beamforming at RIS suffers attenuation from double fading, it offers better asymptotic behaviors than active beamforming at transceivers (e.g., second-order array gain and fourth-order harvested power [10]). Another RIS application is *information modulation* by periodically switching its reflection pattern within the channel coherence time. This creates a free-ride message stream with dual benefits: integrating with legacy transmitter for enhanced channel capacity [11]–[13], or serving as individual source for low-power uplink communication [14]–[16]. Different from above, *channel shaping* exploits RIS as a stand-alone device to modify the inherent properties of the wireless environment, for example, compensate for the Doppler effect [17], flatten frequency-selective channels [18], improve MIMO channel rank [19], and artificially diversify channel over time for orthogonal [20] and non-orthogonal [21] multiple access schemes. This helps to decouple joint beamforming problems into a channel shaping stage and a legacy transceiver design stage, providing a versatile solution for various wireless applications.

B. Related Works

At a specific resource block, channel shaping metrics can be classified into two categories:

- *Singular value:* The impact of RIS has been studied in terms of minimum singular value [22], effective rank [22], [23], condition number [24], [25], and degree of freedom [26]–[28]. Those are closely related to performance measures (e.g., achievable rate and harvested power [29]) but sensitive to minor perturbations of the channel matrix.
- *Power:* The impact of RIS has been studied in terms of channel power gain [2], [30]–[33] in point-to-point channels and leakage interference [34] in interference channels. Those second-order metrics are less informative in MIMO but easier to analyze and optimize.

Although above works offered inspiring glimpses into the channel shaping potential of passive RIS, none attempted to disclose the entire attainable channel singular value region. Most relevant literature [2], [22]–[28], [34] have also been

limited to a Diagonal (D)-RIS model where each element is connected to a dedicated impedance and disconnected from others. As such, wave impinging on one element is entirely scattered by the same element. This simple architecture is modeled by a diagonal scattering matrix with unit-magnitude diagonal entries, which only applies a phase shift to the incoming signal. The idea was soon generalized to Beyond Diagonal (BD)-RIS with group-connected architecture [30], where adjacent elements within the same group are connected via passive reconfigurable components[1]. This allows wave impinging on one element to propagate within the circuit and depart partially from any element in the same group. It can thus manipulate both amplitude and phase of the scattered wave while remaining passive. Such a powerful model can be realized at reduced hardware cost using tree- and forest-connected architectures by graph theory [32]. BD-RIS can also function in multi-sector mode [36] for full-space coverage and multi-user support. Practical challenges such as channel estimation [37], mutual coupling [38], and wideband modelling [39] have also been studied in recent literature. Its beamforming superiority over D-RIS has been proved in Single-Input Single-Output (SISO) and Multiple-Input Single-Output (MISO) systems [30]–[33], [36], [40]–[42], however, the interplay between BD-RIS and MIMO is still in the infancy stage. The authors of [43] investigated the rate-optimal joint beamforming design for a fully-connected BD-RIS-aided MIMO system where the direct channel is negligible. A transmitter-side BD-RIS was introduced to massive MIMO systems that exploits statistical Channel State Information (CSI) for improved spectral efficiency [44], which again assumed negligible direct channel and fully-connected BD-RIS. Received power maximization with continuous-valued and discrete-valued BD-RIS have been tackled respectively in closed form [31] and by machine learning approach [45], but the corresponding single-stream transceiver is rate-suboptimal.

C. Contributions

This paper is motivated by a fundamental question: *What is the singular value (and power gain) shaping capability of a passive RIS in point-to-point MIMO channels?* We aim for a comprehensive answer via analysis and optimization. The contributions are summarized below.

First, we pioneer BD-RIS study in general MIMO channels and interpret its shaping potential as branch matching and mode alignment. Branch matching refers to pairing and combining the branches (i.e., entries) of backward and forward channels associated with each BD-RIS group. Mode alignment refers to aligning and ordering the modes (i.e., singular vectors) of indirect channels with those of direct channel. The former is uniquely attributed to the off-diagonal entries of the scattering matrix of BD-RIS.

Second, we propose a novel BD-RIS design method that allows reshaping of the available channels through singular values manipulation. Our Riemannian Conjugate Gradient (RCG) method compares favorably with respect to existing

ones in that the updates are along the geodesics (i.e., the shortest path between two points in a Riemannian manifold) of the feasible domain to accelerate convergence. It also works for general design problems of group-connected BD-RIS.

Third, we provide a numerical answer to the shaping question by characterizing the Pareto frontiers of channel singular values. The enclosed region generalizes most relevant metrics and provides an intuitive shaping benchmark. Results show that increasing BD-RIS group size enlarges this region, improving the dynamic range of all singular values and the trade-off in manipulating them.

Fourth, we provide an analytical answer to the shaping question in typical deployment scenarios. When the forward/backward channel is rank-deficient, we derive singular value bounds applying to D- and BD-RIS with asymptotically large number of elements. When the direct channel is negligible, we derive singular value bounds applying to fully-connected BD-RIS with arbitrary number of elements. Those bounds are validated by comparing with the numerical results above. Results show that for a fixed number of elements, BD-RIS can approach the asymptotic bounds better than D-RIS.

Fifth, we tackle BD-RIS-aided MIMO rate maximization problem by a local-optimal Alternating Optimization (AO) and a shaping-inspired low-complexity approach. The former iteratively updates active beamforming by eigenmode transmission and passive beamforming by geodesic RCG, until convergence. The latter exploits the BD-RIS to shape the channel for maximum power gain then performs eigenmode transmission. Interestingly, the rate deficit from the shaping-inspired approach diminishes as the BD-RIS evolves towards fully-connected. We conclude that: 1) channel shaping decouples joint beamforming for reduced design complexity; 2) the power and rate gains of BD-RIS over D-RIS increase with the number of scattering elements and MIMO dimensions; 3) at low transmit power, BD-RIS can activate more streams than D-RIS and achieve the asymptotic Degrees of Freedom (DoF), thanks to its higher flexibility of shaping the distribution of channel singular values.

Notation: Italic, bold lower-case, and bold upper-case letters indicate scalars, vectors and matrices, respectively. $\jmath$ denotes the imaginary unit. $\mathbb{C}$ represents the set of complex numbers. $\mathbb{H}^{n \times n}$, $\mathbb{H}^{n \times n}_+$, and $\mathbb{U}^{n \times n}$ denote the set of $n \times n$ Hermitian, positive semi-definite, and unitary matrices, respectively. $\mathbf{0}$ and $\mathbf{I}$ are the all-zero and identity matrices with appropriate size, respectively. $\Re\{\cdot\}$ takes the real part of a complex number. $\mathrm{tr}(\cdot)$ and $\det(\cdot)$ evaluate the trace and determinant of a square matrix, respectively. $\mathrm{diag}(\cdot)$ constructs a square matrix by placing the inputs on the main (block) diagonal and zeros elsewhere. $\mathrm{sv}(\cdot)$ extracts the singular values of a matrix as a non-ascending vector. $\mathrm{card}(\cdot)$ returns the cardinality of a set. $|\cdot|$, $\|\cdot\|$, and $\|\cdot\|_\mathrm{F}$ denote the absolute value, Euclidean norm, and Frobenius norm, respectively. $\sigma_n(\cdot)$ and $\lambda_n(\cdot)$ are the n-th largest singular value and eigenvalue, respectively. $(\cdot)^*$, $(\cdot)^\mathsf{T}$, $(\cdot)^\mathsf{H}$, $(\cdot)^\dagger$ $(\cdot)^{(r)}$, $(\cdot)^\star$ denote the conjugate, transpose, conjugate transpose (Hermitian), Moore-Penrose inverse, r-th iterated point, and stationary point, respectively. $[N]$ is a shortcut for $\{1, 2, ..., N\}$. $(\cdot)_{[x:y]}$ is a shortcut for $(\cdot)_x, (\cdot)_{x+1}, ..., (\cdot)_y$. $\odot$ denotes the element-wise (Hadamard) product. $\mathcal{CN}(\mathbf{0}, \mathbf{\Sigma})$ is the multivariate Circularly Symmetric Complex Gaussian

---

[1]Those components can be either symmetric (e.g., capacitors and inductors) or asymmetric (e.g., ring hybrids and branch-line hybrids) [35], resulting in symmetric and asymmetric scattering matrices, respectively.

(CSCG) distribution with mean $\mathbf{0}$ and covariance $\mathbf{\Sigma}$. $\sim$ means "distributed as".

II. BD-RIS MODEL

Consider a BD-RIS aided point-to-point MIMO system with N_T and N_R transmit and receive antennas, respectively, and N_S scattering elements at the BD-RIS. This configuration is denoted as $N_\mathrm{T} \times N_\mathrm{S} \times N_\mathrm{R}$ throughout the paper. The BD-RIS is modeled as an N_S-port network [46] that divides into G individual groups, where group $g \in [G]$ contains N_g scattering elements interconnected by real-time reconfigurable components [30]. Apparently $N_\mathrm{S} = \sum_{g=1}^{G} N_g$. We assume all groups have the same size $N_g = L \triangleq N_\mathrm{S}/G$, $\forall g$ yet the discussion is extendable to BD-RIS with unequal group size. To establish a theoretical performance bound, we consider a lossless asymmetric[2] BD-RIS without mutual coupling as previously discussed in [36], [43], [47]. The overall scattering matrix of the BD-RIS is block-diagonal

$$\mathbf{\Theta} = \mathrm{diag}(\mathbf{\Theta}_1, ..., \mathbf{\Theta}_G), \tag{1}$$

where $\mathbf{\Theta}_g \in \mathbb{U}^{L \times L}$ is the g-th unitary diagonal block modeling the response of group g. It is noteworthy that the conventional D-RIS is an extreme case of BD-RIS with group size $L=1$. Some potential physical architectures of BD-RIS are illustrated in [30, Fig. 3], [36, Fig. 5], and [32, Fig. 2], where the array geometry and circuit topology has been modeled in the scattering matrix. Let $\mathbf{H}_\mathrm{D} \in \mathbb{C}^{N_\mathrm{R} \times N_\mathrm{T}}$, $\mathbf{H}_\mathrm{B} \in \mathbb{C}^{N_\mathrm{R} \times N_\mathrm{S}}$, $\mathbf{H}_\mathrm{F} \in \mathbb{C}^{N_\mathrm{S} \times N_\mathrm{T}}$ denote the direct (i.e., transmitter-receiver), backward (i.e., RIS-receiver), and forward (i.e., transmitter-RIS) channels, respectively. The equivalent channel depends on the BD-RIS scattering matrix

$$\mathbf{H} = \mathbf{H}_\mathrm{D} + \mathbf{H}_\mathrm{B} \mathbf{\Theta} \mathbf{H}_\mathrm{F} = \mathbf{H}_\mathrm{D} + \sum_g \mathbf{H}_{\mathrm{B},g} \mathbf{\Theta}_g \mathbf{H}_{\mathrm{F},g} \triangleq \mathbf{H}_\mathrm{D} + \sum_g \mathbf{H}_g, \tag{2}$$

where $\mathbf{H}_{\mathrm{B},g} \in \mathbb{C}^{N_\mathrm{R} \times L}$ and $\mathbf{H}_{\mathrm{F},g} \in \mathbb{C}^{L \times N_\mathrm{T}}$ are the backward and forward channels associated with group g, corresponding to the $(g-1)L+1$ to gL columns of $\mathbf{H}_\mathrm{B}$ and rows of $\mathbf{H}_\mathrm{F}$, respectively, and $\mathbf{H}_g \triangleq \mathbf{H}_{\mathrm{B},g} \mathbf{\Theta}_g \mathbf{H}_{\mathrm{F},g}$ is the indirect channel via group g. Since unitary matrices constitute an algebraic group with respect to multiplication, the scattering matrix of group g can be decomposed as

$$\mathbf{\Theta}_g = \mathbf{L}_g \mathbf{R}_g^\mathsf{H}, \tag{3}$$

where $\mathbf{L}_g, \mathbf{R}_g \in \mathbb{U}^{L \times L}$ are two unitary factor matrices. Let $\mathbf{H}_{\mathrm{B},g} = \mathbf{U}_{\mathrm{B},g} \mathbf{\Sigma}_{\mathrm{B},g} \mathbf{V}_{\mathrm{B},g}^\mathsf{H}$ and $\mathbf{H}_{\mathrm{F},g} = \mathbf{U}_{\mathrm{F},g} \mathbf{\Sigma}_{\mathrm{F},g} \mathbf{V}_{\mathrm{F},g}^\mathsf{H}$ be the compact Singular Value Decomposition (SVD) of the backward and forward channels, respectively. The equivalent channel can thus be rewritten as

$$\mathbf{H} = \overbrace{\mathbf{H}_\mathrm{D} + \sum_g \mathbf{U}_{\mathrm{B},g} \mathbf{\Sigma}_{\mathrm{B},g}}^{\text{direct-indirect}} \underbrace{\mathbf{V}_{\mathrm{B},g}^\mathsf{H} \mathbf{L}_g \mathbf{R}_g^\mathsf{H} \mathbf{U}_{\mathrm{F},g}}_{\text{backward-forward}} \mathbf{\Sigma}_{\mathrm{F},g} \mathbf{V}_{\mathrm{F},g}^\mathsf{H}. \tag{4}$$

[2]A symmetric solution can be enforced by projection $\mathbf{\Theta} \leftarrow (\mathbf{\Theta} + \mathbf{\Theta}^\mathsf{T})/2$ if necessary. We will compare the performance of symmetric and asymmetric BD-RIS in Section V.

We observe from (4) that the BD-RIS plays a crucial role in combining backward-forward (intra-group, multiplicative) channels and direct-indirect (inter-group, additive) channels. These two attributes are refined below and discussed in an example.

- *Branch matching:* It refers to pairing and combining the branches (i.e., entries) of $\mathbf{H}_{\mathrm{B},g}$ and $\mathbf{H}_{\mathrm{F},g}$ through unitary transformation $\mathbf{\Theta}_g$.
- *Mode alignment:* It refers to aligning and ordering the modes (i.e., singular vectors) of $\{\mathbf{H}_g\}_{g \in [G]}$ with those of $\mathbf{H}_\mathrm{D}$ through unitary transformations $\{\mathbf{\Theta}_g\}_{g \in [G]}$.

Example 1 (SISO channel gain maximization). *Denote the direct, backward, forward channels as h_D, $\mathbf{h}_\mathrm{B} \in \mathbb{C}^{N_\mathrm{S} \times 1}$, and $\mathbf{h}_\mathrm{F}^\mathsf{H} \in \mathbb{C}^{1 \times N_\mathrm{S}}$, respectively. In this case, mode alignment boils down to phase matching and any $L \in [N_\mathrm{S}]$ (including D-RIS) suffices for perfect alignment between h_D and indirect channels $\{h_g\}_{g \in [G]}$ using*

$$\mathbf{\Theta}_g^{\mathrm{SISO}} = \frac{h_\mathrm{D}}{|h_\mathrm{D}|} \mathbf{V}_{\mathrm{B},g} \mathbf{U}_{\mathrm{F},g}^\mathsf{H}, \quad \forall g, \tag{5}$$

where $\mathbf{V}_{\mathrm{B},g} = [\mathbf{h}_{\mathrm{B},g}/\|\mathbf{h}_{\mathrm{B},g}\|, \ \mathbf{N}_{\mathrm{B},g}] \in \mathbb{U}^{L \times L}$, $\mathbf{U}_{\mathrm{F},g} = [\mathbf{h}_{\mathrm{F},g}/\|\mathbf{h}_{\mathrm{F},g}\|, \ \mathbf{N}_{\mathrm{F},g}] \in \mathbb{U}^{L \times L}$, and $\mathbf{N}_{\mathrm{B},g}, \mathbf{N}_{\mathrm{F},g} \in \mathbb{C}^{L \times (L-1)}$ are the orthonormal bases of null spaces of $\mathbf{h}_{\mathrm{B},g} \in \mathbb{C}^{L \times 1}$ and $\mathbf{h}_{\mathrm{F},g} \in \mathbb{C}^{1 \times L}$, respectively. The corresponding channel gain is a function of L

$$|h|_{\max} = |h_\mathrm{D}| + \sum_g \sum_l |h_{\mathrm{B},g,\pi_{\mathrm{B},g}(l)}||h_{\mathrm{F},g,\pi_{\mathrm{F},g}(l)}|, \tag{6}$$

where $h_{\mathrm{B},g,l}$, $h_{\mathrm{F},g,l}$ are the l-th entries of $\mathbf{h}_{\mathrm{B},g}$ and $\mathbf{h}_{\mathrm{F},g}$, respectively, and $\pi_{\mathrm{B},g}$, $\pi_{\mathrm{F},g}$ are permutations of $[L]$ sorting their magnitude in non-ascending orders. That is, the maximum channel gain is attained when each group, apart from phase shifting, matches the l-th strongest backward and forward channel branches. A larger L provides better branch matching flexibility and can thus grant a higher channel gain.

Example 1 clarifies the difference between branch matching and mode alignment and show their impacts on channel shaping. When it comes to MIMO, the advantage of BD-RIS in branch matching is more pronounced since the number of available branches is proportional to $N_\mathrm{T} N_\mathrm{R}$. On the other hand, the disadvantage of D-RIS in mode alignment deteriorates since each element can only apply a scalar phase shift to the resulting indirect channel of $N \triangleq \min(N_\mathrm{T}, N_\mathrm{R})$ modes.

III. ANALYTICAL BOUNDS ON SINGULAR VALUE SHAPING

In this section, we first provide an example demonstrating the channel shaping advantage of BD-RIS over D-RIS, then derive some analytical bounds related to channel singular values under specific channel conditions.

Example 2 ($2 \times 2 \times 2$ shaping). *Here D-RIS and fully-connected BD-RIS can be modeled by 2 and 4 independent angular parameters, respectively:*

$$\mathbf{\Theta}_\mathrm{D} = \mathrm{diag}(e^{\jmath\theta_1}, e^{\jmath\theta_2}), \quad \mathbf{\Theta}_\mathrm{BD} = e^{\jmath\phi} \begin{bmatrix} e^{\jmath\alpha}\cos\psi & e^{\jmath\beta}\sin\psi \\ -e^{-\jmath\beta}\sin\psi & e^{-\jmath\alpha}\cos\psi \end{bmatrix},$$

We consider a special case where the BD-RIS is symmetric (i.e., $\beta = \pi/2$) and the direct channel is negligible such that ϕ has
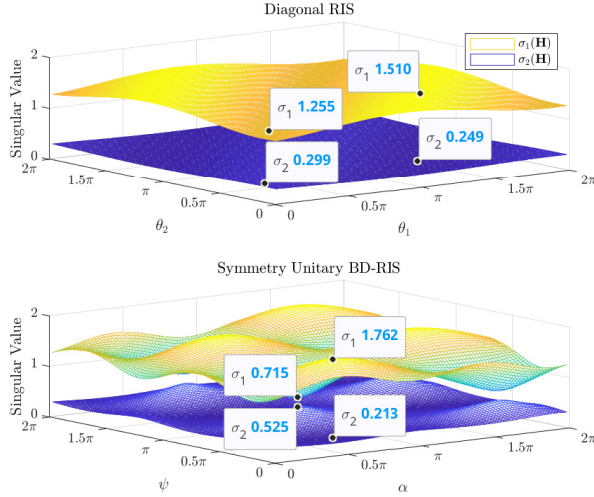
Fig. 1. $2 \times 2 \times 2$ singular value shaping by D-RIS and symmetric fully-connected BD-RIS when the direct channel is negligible. $\sigma_1(\mathbf{H})$ and $\sigma_2(\mathbf{H})$ refer to the most and least dominant singular values, respectively. Their maximum and minimum are marked explicitly on the plot.

no impact on $\mathrm{sv}(\mathbf{H})$, since $\mathrm{sv}(e^{\jmath\phi}\mathbf{A})=\mathrm{sv}(\mathbf{A})$. The singular value shaping capabilities of two RIS architectures can thus be compared visually over 2 tunable parameters. With an exhaustive grid search over (θ_1,θ_2) and (α,ψ), Fig. 1 shows the achievable singular values of a specific channel realization

$$\mathbf{H}_\mathrm{B} = \begin{bmatrix} -0.2059+0.5914\jmath & -0.0909+0.5861\jmath \\ 0.4131+0.2651\jmath & -0.1960+0.4650\jmath \end{bmatrix},$$
$$\mathbf{H}_\mathrm{F} = \begin{bmatrix} -0.6362+0.1332\jmath & -0.1572+1.5538\jmath \\ 0.0196+0.4011\jmath & -0.3170-0.2303\jmath \end{bmatrix}.$$

In this example, both singular values can be manipulated up to[3] $\pm 9\%$ by D-RIS using 2 symmetric components and $\pm 42\%$ by symmetric fully-connected BD-RIS using 3 symmetric components.

Example 2 highlights that the physical grouping of RIS elements, even if using symmetric components, can produce a much wider dynamic range of channel singular values. This motivates analytical and numerical studies on singular value shaping using BD-RIS. A selection of analytical bounds are presented in Propositions $1-3$ and the resulting corollaries.

Definition 1 (Degrees of freedom). *DoF (a.k.a. multiplexing gain) refers to the maximum number of independent streams that can be transmitted in parallel over a MIMO channel, which is defined asymptotically as*

$$d = \lim_{\rho\to\infty} \frac{\log\det(\mathbf{I}+\rho\mathbf{H}\mathbf{H}^\mathsf{H})}{\log\rho}, \tag{7}$$

where ρ is the Signal-to-Noise Ratio (SNR).

Proposition 1 (Degrees of freedom). *In point-to-point MIMO, BD-RIS cannot achieve a larger number of DoF than D-RIS.*

Proof. Please refer to Appendix A. □

[3]The percentage for manipulating $\sigma_n(\mathbf{H})$ is calculated by $\eta_n^+ = \frac{\max\sigma_n(\mathbf{H})-\mathrm{avg}\sigma_n(\mathbf{H})}{\mathrm{avg}\sigma_n(\mathbf{H})}\times 100\%$ and $\eta_n^- = \frac{\min\sigma_n(\mathbf{H})-\mathrm{avg}\sigma_n(\mathbf{H})}{\mathrm{avg}\sigma_n(\mathbf{H})}\times 100\%$.

Proposition 1 suggests that we cannot hope for a DoF gain (i.e., more parallel channels) by simply connecting the RIS elements. We thus focus on the question of reshaping the available channels through manipulation of the singular values.

Proposition 2 (Rank-deficient channel). *If the minimum rank of backward and forward channels is k ($k \leq N$), then for D-RIS or BD-RIS of arbitrary number of elements, the n-th singular value of the equivalent channel is bounded above and below respectively by*

$$\sigma_n(\mathbf{H}) \leq \sigma_{n-k}(\mathbf{T}), \qquad \text{if } n > k, \tag{8a}$$
$$\sigma_n(\mathbf{H}) \geq \sigma_n(\mathbf{T}), \qquad \text{if } n < N-k+1, \tag{8b}$$

where $\mathbf{T}$ is arbitrary auxiliary matrix satisfying

$$\mathbf{T}\mathbf{T}^\mathsf{H} = \begin{cases} \mathbf{H}_\mathrm{D}(\mathbf{I}-\mathbf{V}_\mathrm{F}\mathbf{V}_\mathrm{F}^\mathsf{H})\mathbf{H}_\mathrm{D}^\mathsf{H}, & \text{if } \mathrm{rank}(\mathbf{H}_\mathrm{F})=k, \\ \mathbf{H}_\mathrm{D}^\mathsf{H}(\mathbf{I}-\mathbf{U}_\mathrm{B}\mathbf{U}_\mathrm{B}^\mathsf{H})\mathbf{H}_\mathrm{D}, & \text{if } \mathrm{rank}(\mathbf{H}_\mathrm{B})=k, \end{cases} \tag{9}$$

and $\mathbf{V}_\mathrm{F}$ and $\mathbf{U}_\mathrm{B}$ are the right and left compact singular matrices of $\mathbf{H}_\mathrm{F}$ and $\mathbf{H}_\mathrm{B}$, respectively.

Proof. Please refer to Appendix B. □

Inequality (8a) states that if $\mathbf{H}_\mathrm{B}$ and $\mathbf{H}_\mathrm{F}$ are at least rank k, then the n-th singular value of $\mathbf{H}$ can be enlarged to the $(n-k)$-th singular value of $\mathbf{T}$, or suppressed to the n-th singular value of $\mathbf{T}$. Moreover, the first k channel singular values are unbounded above[4] while the last k channel singular values can be suppressed to zero. A special case is Corollary 2.1 for Line-of-Sight (LoS) channel[5].

Corollary 2.1 (LoS channel). *If at least one of backward and forward channels is LoS, then a D-RIS or BD-RIS can at most enlarge the n-th ($n \geq 2$) channel singular value to the $(n-1)$-th singular value of $\mathbf{T}$, or suppress the n-th channel singular value to the n-th singular value of $\mathbf{T}$. That is,*

$$\sigma_1(\mathbf{H}) \geq \sigma_1(\mathbf{T}) \geq \sigma_2(\mathbf{H}) \geq ... \geq \sigma_{N-1}(\mathbf{T}) \geq \sigma_N(\mathbf{H}) \geq \sigma_N(\mathbf{T}). \tag{10}$$

Proof. This is a direct result of (8) with $k=1$. □

We emphasize that Proposition 2 and Corollary 2.1 apply to both D- and BD-RIS configurations regardless of the status of the direct channel. Out of $2N$ bounds in (8) or (10), N of them can be *simultaneously* tight as N_S goes to infinity, namely, when the direct channel becomes negligible[6]. For a finite N_S, the RIS may prioritize a subset of those by aligning the corresponding modes, and we will later show by simulation that BD-RIS outperforms D-RIS on this purpose. Proposition 2 provides a reference on the selection of N_S in low-multipath application scenarios. Next, we shift the focus to another popular RIS deployment scenario where the direct channel is blocked.

[4]The energy conservation law $\sum_n \sigma_n^2(\mathbf{H}) \leq 1$ still has to be respected in all cases. This constraint is omitted in context for brevity.

[5]A similar eigenvalue result has been derived for D-RIS only [48].

[6]Negligible direct channel refers to the case where the power of the signal arriving at the receiver through the direct path is negligible compared to that through the scattering of RIS, i.e., $\mathbf{H} \approx \sum_g \mathbf{H}_g$. This can result from a very large number of RIS elements (as discussed in Proposition 2) or physical obstacles in the propagation path (as discussed in Proposition 3).

Proposition 3 (Negligible direct channel). *If the direct channel is negligible, then a fully-connected BD-RIS can manipulate the channel singular values up to*

$$\mathrm{sv}(\mathbf{H}) = \mathrm{sv}(\mathbf{BF}), \tag{11}$$

where $\mathbf{B}$ *and* $\mathbf{F}$ *are arbitrary matrices with* $\mathrm{sv}(\mathbf{B}) = \mathrm{sv}(\mathbf{H}_\mathrm{B})$ *and* $\mathrm{sv}(\mathbf{F}) = \mathrm{sv}(\mathbf{H}_\mathrm{F})$.

Proof. Please refer to Appendix C. □

Proposition 3 says that if the direct channel is negligible and the BD-RIS is fully-connected, the only singular value bounds on the equivalent channel are those on the product of unitary-transformed backward and forward channels. It is *not necessarily* an asymptotic result and does *not* depend on any relationship between N_R, N_S, and N_T. Its importance lies in the fact that the channel shaping question in Section I-C can be recast as a linear algebra question: *How the singular values of matrix product are bounded by the singular values of its individual factors?* The question is partially answered in Corollaries 3.1 – 3.4 over the notation[7] $\bar{N} = \max(N_\mathrm{T}, N_\mathrm{S}, N_\mathrm{R})$ and $\sigma_n(\mathbf{H}) = \sigma_n(\mathbf{H}_\mathrm{F}) = \sigma_n(\mathbf{H}_\mathrm{B}) = 0$ for $n \in [\bar{N}] \backslash [N]$. These results are by no means complete and interested readers are referred to [49, Chapter 16, 24] and [50, Chapter 3] for more information.

Corollary 3.1 (Product of subset of singular values). *The product of subset of singular values of* $\mathbf{H}$ *is bounded from above by those of* $\mathbf{H}_\mathrm{B}$ *and* $\mathbf{H}_\mathrm{F}$, *that is,*

$$\prod_{k \in K} \sigma_k(\mathbf{H}) \le \prod_{i \in I} \sigma_i(\mathbf{H}_\mathrm{B}) \prod_{j \in J} \sigma_j(\mathbf{H}_\mathrm{F}), \tag{12}$$

for all admissible triples $(I, J, K) \in T_r^{\bar{N}}$ *with* $r < \bar{N}$, *where*

$$T_r^{\bar{N}} \triangleq \Big\{ (I, J, K) \in U_r^{\bar{N}} \,\big|\, \forall p < r,\, \forall (F, G, H) \in T_p^r,$$
$$\sum_{f \in F} i_f + \sum_{g \in G} j_g \le \sum_{h \in H} k_h + \frac{p(p+1)}{2} \Big\},$$

$$U_r^{\bar{N}} \triangleq \Big\{ (I, J, K) \subseteq [\bar{N}]^3 \,\big|\, \sum_{i \in I} i + \sum_{j \in J} j = \sum_{k \in K} k + \frac{r(r+1)}{2} \Big\}.$$

Proof. Please refer to [51, Theorem 8]. □

Corollary 3.1, also recognized as a variation of Horn's inequality [52], is one of the most comprehensive result under the assumption of Proposition 3 (i.e., negligible direct channel and fully-connected BD-RIS). The number of admissible triples increases exponentially with $\bar{N}$ despite some resulting inequalities can be redundant. Apart from upper bounds, (12) can also induce lower bounds on channel singular values. Those facts render the shaping limit analysis non-trivial for massive RIS-aided MIMO systems. Below we showcase some useful results that can be derived from Corollary 3.1.

Corollary 3.2 (Product of some largest or smallest singular values). *The product of the first (resp. last) k singular values*

[7]This is equivalent to padding zero blocks at the end of $\mathbf{H}$, $\mathbf{H}_\mathrm{B}$, and $\mathbf{H}_\mathrm{F}$ to make square matrices, which generalizes relevant results to non-square case.

of $\mathbf{H}$ *is bounded from above (resp. below) by those of* $\mathbf{H}_\mathrm{B}$ *and* $\mathbf{H}_\mathrm{F}$, *that is,*

$$\prod_{n=1}^{k} \sigma_n(\mathbf{H}) \le \prod_{n=1}^{k} \sigma_n(\mathbf{H}_\mathrm{B}) \sigma_n(\mathbf{H}_\mathrm{F}), \tag{13a}$$

$$\prod_{n=\bar{N}}^{\bar{N}-k+1} \sigma_n(\mathbf{H}) \ge \prod_{n=\bar{N}}^{\bar{N}-k+1} \sigma_n(\mathbf{H}_\mathrm{B}) \sigma_n(\mathbf{H}_\mathrm{F}). \tag{13b}$$

Proof. Please refer to and Appendix D. □

Corollary 3.3 (Individual singular value). *The n-th channel singular value can be manipulated up to*

$$\max_{i+j=n+\bar{N}} \sigma_i(\mathbf{H}_\mathrm{B}) \sigma_j(\mathbf{H}_\mathrm{F}) \le \sigma_n(\mathbf{H}) \le \min_{i+j=n+1} \sigma_i(\mathbf{H}_\mathrm{B}) \sigma_j(\mathbf{H}_\mathrm{F}), \tag{14}$$

where $(i, j) \in [\bar{N}]^2$. *The upper and lower bounds are attained respectively at*

$$\boldsymbol{\Theta}_{\mathrm{sv}\text{-}n\text{-max}}^{\mathrm{MIMO\text{-}ND}} = \mathbf{V}_\mathrm{B} \mathbf{L} \mathbf{P} \mathbf{R} \mathbf{U}_\mathrm{F}^\mathsf{H}, \tag{15a}$$
$$\boldsymbol{\Theta}_{\mathrm{sv}\text{-}n\text{-min}}^{\mathrm{MIMO\text{-}ND}} = \mathbf{V}_\mathrm{B} \mathbf{L} \mathbf{Q} \mathbf{R} \mathbf{U}_\mathrm{F}^\mathsf{H}, \tag{15b}$$

where $\mathbf{V}_\mathrm{B}, \mathbf{U}_\mathrm{F} \in \mathbb{U}^{N_\mathrm{S} \times N_\mathrm{S}}$ *are the right and left singular matrices of* $\mathbf{H}_\mathrm{B}$ *and* $\mathbf{H}_\mathrm{F}$, *respectively,* $\mathbf{L}, \mathbf{R}$ *are arbitrary block-diagonal unitary matrices with size of block* $n \in [N_\mathrm{S}]$ *equal to the multiplicity of* $\sigma_n(\mathbf{H}_\mathrm{B})$ *and* $\sigma_n(\mathbf{H}_\mathrm{B})$, *respectively, and* $\mathbf{P}$ *and* $\mathbf{Q}$ *are arbitrary doubly stochastic matrices of dimension* N_S *satisfying:*

- *The* (i, j)-*th entries sum up to 1, where*

$$(i, j) = \begin{cases} \underset{i+j=n+1}{\mathrm{argmin}}\, \sigma_i(\mathbf{H}_\mathrm{B}) \sigma_j(\mathbf{H}_\mathrm{F}) \triangleq \mathcal{S}_n(\mathbf{P}) & \text{for } \mathbf{P}, \\ \underset{i+j=n+\bar{N}}{\mathrm{argmax}}\, \sigma_i(\mathbf{H}_\mathrm{B}) \sigma_j(\mathbf{H}_\mathrm{F}) \triangleq \mathcal{S}_n(\mathbf{Q}) & \text{for } \mathbf{Q}; \end{cases}$$

- *The submatrix with* i-*th rows and* j-*th columns deleted,* $(i, j) \in \mathcal{S}_n$, *denoted as* $\mathbf{Y}$, *is arbitrary doubly stochastic matrix of dimension* $N_\mathrm{S} - \mathrm{card}(\mathcal{S}_n)$ *satisfying*

$$\sigma_{n-1}(\hat{\boldsymbol{\Sigma}}_\mathrm{B} \mathbf{Y} \hat{\boldsymbol{\Sigma}}_\mathrm{F}) \ge \min_{i+j=n+1} \sigma_i(\mathbf{H}_\mathrm{B}) \sigma_j(\mathbf{H}_\mathrm{F}) \quad \text{for } \mathbf{P},$$
$$\sigma_{n+1}(\hat{\boldsymbol{\Sigma}}_\mathrm{B} \mathbf{Y} \hat{\boldsymbol{\Sigma}}_\mathrm{F}) \le \max_{i+j=n+\bar{N}} \sigma_i(\mathbf{H}_\mathrm{B}) \sigma_j(\mathbf{H}_\mathrm{F}) \quad \text{for } \mathbf{Q},$$

where $\hat{\boldsymbol{\Sigma}}_\mathrm{B}$ *and* $\hat{\boldsymbol{\Sigma}}_\mathrm{F}$ *are diagonal singular value matrices of* $\mathbf{H}_\mathrm{B}$ *and* $\mathbf{H}_\mathrm{F}$ *with the* i-*th rows and* j-*th columns deleted,* $(i, j) \in \mathcal{S}_n$.

Proof. In (14), the set of upper bounds

$$\big\{ \sigma_n(\mathbf{H}) \le \sigma_i(\mathbf{H}_\mathrm{B}) \sigma_j(\mathbf{H}_\mathrm{F}) \,\big|\, [i, j, k] \in [\bar{N}]^3, i+j=n+1 \big\} \tag{16}$$

is a special case of (12) with $(I, J, K) \in [\bar{N}]^3$. The minimum[8] of (16) is selected as the tightest upper bound in (14). On the other hand, the set of lower bounds

$$\big\{ \sigma_n(\mathbf{H}) \ge \sigma_i(\mathbf{H}_\mathrm{B}) \sigma_j(\mathbf{H}_\mathrm{F}) \,\big|\, [i, j, k] \in [\bar{N}]^3, i+j=n+\bar{N} \big\} \tag{17}$$

can be induced by (16), (55), and the non-negativity of singular values. The maximum of (17) is selected as the tightest lower bound in (14).

[8]One may think to take the *maximum* of those upper bounds as the problem of interest is the attainable dynamic range of n-th singular value. However, this is infeasible since the singular values will be reordered therein.

To attain the upper bound, the BD-RIS needs to maximize the minimum of the first n singular values of $\mathbf{H}$. It follows from (15a) that

$$\begin{aligned}
\mathrm{sv}(\mathbf{H}) &= \mathrm{sv}(\mathbf{H}_B \mathbf{V}_B \mathbf{P} \boldsymbol{\Theta}_D \mathbf{U}_F^H \mathbf{H}_F) \\
&= \mathrm{sv}(\mathbf{U}_B \boldsymbol{\Sigma}_B \mathbf{P} \boldsymbol{\Theta}_D \boldsymbol{\Sigma}_F \mathbf{U}_F^H) \\
&= \mathrm{sv}(\mathbf{U}_B \boldsymbol{\Sigma}_B \mathbf{P} \boldsymbol{\Sigma}_F \boldsymbol{\Theta}_D \mathbf{U}_F^H) \\
&= \mathrm{sv}(\boldsymbol{\Sigma}_B \mathbf{P} \boldsymbol{\Sigma}_F)
\end{aligned}$$

where $\mathbf{H}_B = \mathbf{U}_B \boldsymbol{\Sigma}_B \mathbf{V}_B^H$ and $\mathbf{H}_F = \mathbf{U}_F \boldsymbol{\Sigma}_F \mathbf{V}_F^H$.

The doubly stochastic matrix $\mathbf{P}$ should align the modes of $\mathbf{H}_B$ and $\mathbf{H}_F$ such that the first n modes of $\mathbf{H}$ are maximized.

One feasible solution is to align and order the first n modes of $\mathbf{H}_B$ and $\mathbf{H}_F$, resulting in $\sigma_n(\mathbf{H}) = \min_{i+j=n+1} \sigma_i(\mathbf{H}_B)\sigma_j(\mathbf{H}_F)$. If such (i,j) pairs are not unique, then any mixture of them would produce the same result. However, since we only care about the n-th singular value, the first $n-1$ singular values can be arbitrarily reordered.

proper matching of the first n modes of $\mathbf{H}_B$ to the first n modes of $\mathbf{H}_F$. In particular, mode i of $\mathbf{H}_B$ should be completely aligned with mode j of $\mathbf{H}_F$ where $(i,j) = \mathrm{argmin}_{i+j=n+1} \sigma_i(\mathbf{H}_B)\sigma_j(\mathbf{H}_F)$ for $\mathbf{P}$

$\square$

Now we can see the alignment by $V_B \ U_F$ and ordering by $P \ Q$.

We highlight the solution (15) is not unique.

In particular, the extreme singular values can be manipulated up to

$$\max_{i+j=n+1} \sigma_i(\mathbf{H}_B)\sigma_j(\mathbf{H}_F) \leq \sigma_1(\mathbf{H}) \leq \sigma_1(\mathbf{H}_B)\sigma_1(\mathbf{H}_F), \quad (18a)$$

$$\min_{i+j=n+1} \sigma_i(\mathbf{H}_B)\sigma_j(\mathbf{H}_F) \geq \sigma_{\bar{N}}(\mathbf{H}) \geq \sigma_{\bar{N}}(\mathbf{H}_B)\sigma_{\bar{N}}(\mathbf{H}_F), \quad (18b)$$

where the arguments of $\max$ and $\min$ are essentially $\sigma_1(\mathbf{H}_B)\sigma_{\bar{N}}(\mathbf{H}_F), \sigma_2(\mathbf{H}_B)\sigma_{\bar{N}-1}(\mathbf{H}_F), ..., \sigma_{\bar{N}}(\mathbf{H}_B)\sigma_1(\mathbf{H}_F)$. We notice that the right side inequalities in (18a) and (18b) are special cases of (13a) and (13b) when $k=1$, respectively. It is evident from (14) that to enlarge the n-th singular value of $\mathbf{H}$, one should

enumerate all matching pairs $(i,j) \in [\bar{N}]^2 \,|\, i+j=n+1$, find the one with the minimum product singular value

match the singular

align the i-th singular value of $\mathbf{H}_B$ with the j-th singular value of $\mathbf{H}_F$ such that $i+j = n+\bar{N}$.

Corollary 3.4 (Channel power gain). *The channel power gain is bounded from above (resp. below) by the inner product of squared singular values of $\mathbf{H}_B$ and $\mathbf{H}_F$ when they are sorted similarly (resp. oppositely), that is,*

$$\sum_n \sigma_n^2(\mathbf{H}_B)\sigma_{N_S-n+1}^2(\mathbf{H}_F) \leq \|\mathbf{H}\|_F^2 \leq \sum_n \sigma_n^2(\mathbf{H}_B)\sigma_n^2(\mathbf{H}_F), \quad (19)$$

whose[9] upper and lower bounds are attained respectively at

$$\boldsymbol{\Theta}_{P\text{-}max}^{MIMO\text{-}ND} = \mathbf{V}_B \boldsymbol{\Theta}_D \mathbf{U}_F^H, \quad (20a)$$

$$\boldsymbol{\Theta}_{P\text{-}min}^{MIMO\text{-}ND} = \mathbf{V}_B \mathbf{J} \boldsymbol{\Theta}_D \mathbf{U}_F^H, \quad (20b)$$

---

[9]As a side note, we notice [53] discussed a similar bound using extreme singular values $\max(\sigma_{\bar{N}}(\mathbf{H}_B)\|\mathbf{H}_F\|_F^2, \sigma_{\bar{N}}(\mathbf{H}_F)\|\mathbf{H}_B\|_F^2) \leq \|\mathbf{H}\|_F^2 \leq \min(\sigma_1(\mathbf{H}_B)\|\mathbf{H}_F\|_F^2, \sigma_1(\mathbf{H}_F)\|\mathbf{H}_B\|_F^2)$. This is a looser version of (19) and cannot take equalities unless the extreme singular values are of multiplicity $\bar{N}$.

where $\mathbf{J}$ is the exchange (a.k.a. backward identity) matrix of dimension N_S.

Proof. Please refer to Appendix F. $\square$

Example 3 (Bounds on $3 \times 3 \times 3$ shaping). *Consider a $3 \times 3 \times 3$ setup with negligible direct channel. Let $\mathbf{H}_B = \mathrm{diag}(4,5,6)$, $\mathbf{H}_F = \mathrm{diag}(3,1,2)$. Apparently any D-RIS can only achieve $\mathrm{sv}(\mathbf{H}) = [12,12,5]^T$ due to limited branch matching capability. On the other hand, Corollary 3.1 suggests that a fully-connected BD-RIS can manipulate the singular values up to*

$$\sigma_1(\mathbf{H}) \leq \sigma_1(\mathbf{H}_B)\sigma_1(\mathbf{H}_F), \quad \sigma_2(\mathbf{H}) \leq \sigma_1(\mathbf{H}_B)\sigma_2(\mathbf{H}_F)$$
$$\sigma_2(\mathbf{H}) \leq \sigma_2(\mathbf{H}_B)\sigma_1(\mathbf{H}_F), \quad \sigma_3(\mathbf{H}) \leq \sigma_1(\mathbf{H}_B)\sigma_3(\mathbf{H}_F)$$
$$\sigma_3(\mathbf{H}) \leq \sigma_3(\mathbf{H}_B)\sigma_1(\mathbf{H}_F), \quad \sigma_3(\mathbf{H}) \leq \sigma_2(\mathbf{H}_B)\sigma_2(\mathbf{H}_F)$$

while a BD-RIS $\boldsymbol{\Theta} = \begin{bmatrix} 0 & 1 \\ 1 & 0 \end{bmatrix}$ can match the stronger branches by unitary transformation to achieve $\mathrm{sv}(\mathbf{H}) = [12,2]^T$. The bounds on individual singular values are $8 \leq \sigma_1(\mathbf{H}) \leq 12$ and $2 \leq \sigma_2(\mathbf{H}) \leq 3$. However, the upper/lower bounds are not simultaneously achievable due to the trade-off between two modes.

Example 3 shows that a fully-connected BD-RIS can apply right unitary transformation on $\mathbf{H}_B$ and left unitary transformation on $\mathbf{H}_F$ That is, fully-connected BD-RIS applies right unitary transformation on $\mathbf{H}_B$ and left unitary transformation on $\mathbf{H}_F$, widening the singular values to $8 \leq \sigma_1(\mathbf{H}) \leq 12$ and $2 \leq \sigma_2(\mathbf{H}) \leq 3$.

All equalities achieved by perfect alignment of all modes.

To achieve equalities in Corollaries **??** – 3.4, the RIS needs to completely align the singular vector spaces of $\mathbf{H}_B$ and $\mathbf{H}_F$. The resulting scattering matrix is generally required to be unitary

$$\boldsymbol{\Theta}^\star = \mathbf{V}_B \mathbf{U}_F^H, \quad (21)$$

which can be concluded from (53) and (54) in Appendix C. We notice that D-RIS can attain those equalities if and only if $\mathbf{H}_B$ and $\mathbf{H}_F$ are both rank-1. In such case, the equivalent channel reduces to $\mathbf{H} = \sigma_B \sigma_F \mathbf{u}_B \mathbf{v}_B^H \boldsymbol{\Theta} \mathbf{u}_F \mathbf{v}_F^H$ and the RIS only needs to align $\mathbf{v}_B^H$ and $\mathbf{u}_F$ by

$$\boldsymbol{\Theta}^\star = \mathbf{v}_B \mathbf{u}_F^H \odot \mathbf{I}, \quad (22)$$

which reduces to a special case of (5) with $L=1$. However, in general D-RIS is not sufficient to achieve the upper bound of channel power gain. This again highlights the benefit of BD-RIS in reshaping available channels.

As a side note, when both $\mathbf{H}_B$ and $\mathbf{H}_F$ follow Rayleigh fading, the maximum expected channel power gain can be numerically evaluated as

$$\mathbb{E}\{\|\mathbf{H}\|_F^2\} = \sum_n \int_0^\infty f_{\lambda_n^{\min(N_R,N_S)}}(x)dx \int_0^\infty f_{\lambda_n^{\min(N_S,N_T)}}(x)dx, \quad (23)$$

where λ_n^K is the n-th eigenvalue of the complex $K \times K$ Wishart matrix with probability density function $f_{\lambda_n^K}(x)$ given by [54, Equation 51]. We note that (23) generalizes the SISO power gain attainable by BD-RIS [30, Equation 58] to MIMO and models the contribution of transmit and receive antennas under double Rayleigh fading. In Section V, we will

numerically evaluate the channel power gain and compare it with the theoretical upper bound.

Proposition 3 and Corollaries 3.1 – 3.4 provide a comprehensive answer to the shaping capability question in terms of singular value bounds and channel power gain limits. Extending those results to the case of direct channel is non-trivial since the singular vector spaces of direct-indirect channels and backward-forward channels cannot be aligned at the same time. In such case, we can invoke optimization approaches from a singular value perspective (discussed in Section IV-C) or a power gain perspective (to be discussed in Section IV-D).

IV. BD-RIS DESIGN FRAMEWORKS

This section aims for an efficient yet universal optimization framework for group-connected BD-RIS design. Most relevant optimization problems can be formulated as

$$\max_{\boldsymbol{\Theta}} \quad f(\boldsymbol{\Theta}) \tag{24a}$$

$$\text{s.t.} \quad \boldsymbol{\Theta}_g^{\mathsf{H}} \boldsymbol{\Theta}_g = \mathbf{I}, \quad \forall g, \tag{24b}$$

where the objective function $f(\boldsymbol{\Theta})$ is a function of the BD-RIS scattering matrix, for example, channel singular value (to be discussed in Section IV-C), channel power gain (to be discussed in Section IV-D), and achievable rate (to be discussed in Section IV-E). The feasible domain of each group is a L-dimensional Stiefel manifold $\boldsymbol{\Theta}_g \in \mathbb{U}^{L \times L}$ that is non-convex and non-Euclidean. Therefore, most BD-RIS optimization problems are solved by *relax-then-project* methods [40] or *general manifold RCG* [36], [41], [47]. The former solves unconstrained problem (24a) by quasi-Newton methods then projects the solution back to domain 24b, which often ends up far from optimal. The latter generalizes the conjugate gradient methods to Riemannian manifolds and iteratively updates the solution by addition and retraction. In the following context, we briefly review the general RCG method and discuss its drawbacks inherited from the non-geodesic nature, then propose a novel group-wise geodesic RCG method that operates directly on the Stiefel manifold for faster convergence.

A. General (Non-Geodesic) RCG

A geodesic is a curve representing the shortest path between two points in a Riemannian manifold, whose tangent vectors remain parallel when transporting along the curve. The general RCG method proposed in [55], [56] is applicable to optimization problems over arbitrary manifolds. The idea is to perform additive updates along the conjugate direction guided by the Riemannian gradient, project the solution back onto the manifold, and repeat until convergence. For optimization problem (24), the steps for BD-RIS group g at iteration r are summarized below:

1) *Compute the Euclidean gradient:* The gradient of f with respect to $\boldsymbol{\Theta}_g^*$ in the Euclidean space is

$$\nabla_{\mathrm{E},g}^{(r)} = \frac{\partial f(\boldsymbol{\Theta}_g^{(r)})}{\partial \boldsymbol{\Theta}_g^*}; \tag{25}$$

2) *Translate to the Riemannian gradient [55]:* At point $\boldsymbol{\Theta}^{(r)}$, the Riemannian gradient lies in the tangent space of the

Stiefel manifold $\mathcal{T}_{\boldsymbol{\Theta}_g^{(r)}} \mathbb{U}^{L \times L} \triangleq \{\mathbf{M} \in \mathbb{C}^{L \times L} \,|\, \mathbf{M}^{\mathsf{H}} \boldsymbol{\Theta}_g^{(r)} + \boldsymbol{\Theta}_g^{(r)\mathsf{H}} \mathbf{M} = \mathbf{0}\}$. It gives the steepest ascent direction of the objective on the manifold can be obtained by projecting the Euclidean gradient onto the tangent space:

$$\nabla_{\mathrm{R},g}^{(r)} = \nabla_{\mathrm{E},g}^{(r)} - \boldsymbol{\Theta}_g^{(r)} \nabla_{\mathrm{E},g}^{(r)\mathsf{H}} \boldsymbol{\Theta}_g^{(r)}; \tag{26}$$

3) *Determine the conjugate direction [57]:* The conjugate direction is obtained over the Riemannian gradient and previous direction as

$$\mathbf{D}_g^{(r)} = \nabla_{\mathrm{R},g}^{(r)} + \gamma_g^{(r)} \mathbf{D}_g^{(r-1)}, \tag{27}$$

where $\gamma_g^{(r)}$ is the parameter that deviates the conjugate direction from the tangent space for accelerated convergence. A popular choice is the Polak-Ribière formula

$$\gamma_g^{(r)} = \frac{\mathrm{tr}\big((\nabla_{\mathrm{R},g}^{(r)} - \nabla_{\mathrm{R},g}^{(r-1)}) \nabla_{\mathrm{R},g}^{(r)\mathsf{H}}\big)}{\mathrm{tr}\big(\nabla_{\mathrm{R},g}^{(r-1)} \nabla_{\mathrm{R},g}^{(r-1)\mathsf{H}}\big)}; \tag{28}$$

4) *Perform additive update [56]:* The point is updated by moving along a straight path in the conjugate direction

$$\bar{\boldsymbol{\Theta}}_g^{(r+1)} = \boldsymbol{\Theta}_g^{(r)} + \mu \mathbf{D}_g^{(r)}, \tag{29}$$

where μ is the step size refinable by the Armijo rule [58];

5) *Retract for feasibility [47], [55]:* The resulting point needs to be projected to the closest point (in terms of Euclidean distance) on the Stiefel manifold by

$$\boldsymbol{\Theta}_g^{(r+1)} = \bar{\boldsymbol{\Theta}}_g^{(r+1)} \big(\bar{\boldsymbol{\Theta}}_g^{(r+1)\mathsf{H}} \bar{\boldsymbol{\Theta}}_g^{(r+1)}\big)^{-1/2}. \tag{30}$$

One can also combine the addition (29) and retraction (30) in one step

$$\boldsymbol{\Theta}_g^{(r+1)} = \big(\boldsymbol{\Theta}_g^{(r)} + \mu \mathbf{D}_g^{(r)}\big) \big(\mathbf{I} + \mu^2 \mathbf{D}_g^{(r)\mathsf{H}} \mathbf{D}_g^{(r)}\big)^{-1/2}, \tag{31}$$

and determine the step size therein.

The method is called non-geodesic since the addition (29) and retraction (30) constitute a zigzag path departing from and returning to the manifold. It converges to stationary points of the original problem but usually requires a large number of iterations due to inefficient operations in the Euclidean space.

B. Geodesic RCG

Before introducing geodesic RCG, we revisit some basic concepts in differential geometry. A Lie group is simultaneously a continuous group and a differentiable manifold. Lie algebra refers to the tangent space of the Lie group at the identity element. The exponential map acts as a bridge between the Lie algebra and Lie group, which allows one to recapture the local group structure using linear algebra techniques. The set of unitary matrices $\mathbb{U}^{L \times L}$ forms a Lie group $U(L)$ under multiplication, and the corresponding Lie algebra $\mathfrak{u}(L) \triangleq \mathcal{T}_{\mathbf{I}} \mathbb{U}^{L \times L} = \{\mathbf{M} \in \mathbb{C}^{L \times L} \,|\, \mathbf{M}^{\mathsf{H}} + \mathbf{M} = \mathbf{0}\}$ consists of skew-Hermitian matrices. A geodesic emanating from the identity with velocity $\mathbf{D} \in \mathfrak{u}(L)$ can be described by [59]

$$\mathbf{G}_{\mathbf{I}}(\mu) = \exp(\mu \mathbf{D}), \tag{32}$$

where $\exp(\mathbf{A}) = \sum_{k=0}^{\infty} (\mathbf{A}^k / k!)$ is the matrix exponential and μ is the step size (i.e., magnitude of the tangent vector). Note

Algorithm 1: Group-wise geodesic RCG for BD-RIS design

Input: $f(\boldsymbol{\Theta})$, G
Output: $\boldsymbol{\Theta}^\star$
1: **Initialize** $r \leftarrow 0$, $\boldsymbol{\Theta}^{(0)}$
2: **Repeat**
3:     **For** $g \leftarrow 1$ to G
4:         $\nabla_{\mathrm{E},g}^{(r)} \leftarrow$ (25)
5:         $\tilde{\nabla}_{\mathrm{R},g}^{(r)} \leftarrow$ (34)
6:         $\tilde{\gamma}_g^{(r)} \leftarrow$ (35)
7:         $\mathbf{D}_g^{(r)} \leftarrow$ (36)
8:         **If** $\Re\{\mathrm{tr}(\mathbf{D}_g^{(r)\mathsf{H}}\tilde{\nabla}_{\mathrm{R},g}^{(r)})\} < 0$ ▷ not an ascent direction
9:             $\mathbf{D}_g^{(r)} \leftarrow \tilde{\nabla}_{\mathrm{R},g}^{(r)}$
10:         **End If**
11:         $\mu \leftarrow 1$
12:         $\mathbf{G}_g^{(r)}(\mu) \leftarrow$ (33)
13:         **While** $f(\mathbf{G}_g^{(r)}(2\mu)) - f(\boldsymbol{\Theta}_g^{(r)}) \geq \mu \cdot \mathrm{tr}(\mathbf{D}_g^{(r)}\mathbf{D}_g^{(r)\mathsf{H}})/2$
14:             $\mu \leftarrow 2\mu$
15:         **End While**
16:         **While** $f(\mathbf{G}_g^{(r)}(\mu)) - f(\boldsymbol{\Theta}_g^{(r)}) < \mu/2 \cdot \mathrm{tr}(\mathbf{D}_g^{(r)}\mathbf{D}_g^{(r)\mathsf{H}})/2$
17:             $\mu \leftarrow \mu/2$
18:         **End While**
19:         $\boldsymbol{\Theta}_g^{(r+1)} \leftarrow$ (37)
20:     **End For**
21:     $r \leftarrow r+1$
22: **Until** $|f(\boldsymbol{\Theta}^{(r)}) - f(\boldsymbol{\Theta}^{(r-1)})|/f(\boldsymbol{\Theta}^{(r-1)}) \leq \epsilon$

---

that the right translation is an isometry in $U(L)$. During the optimization of group g, the geodesic evaluated at the identity (32) should be translated to $\boldsymbol{\Theta}_g^{(r)}$ for successive updates [60]

$$\mathbf{G}_g^{(r)}(\mu) = \mathbf{G}_{\mathbf{I}}(\mu)\boldsymbol{\Theta}_g^{(r)} = \exp(\mu\mathbf{D}_g^{(r)})\boldsymbol{\Theta}_g^{(r)}, \qquad (33)$$

while the Riemannian gradient evaluated at $\boldsymbol{\Theta}_g^{(r)}$ (26) should be translated back to the identity for exploiting the Lie algebra [60]

$$\tilde{\nabla}_{\mathrm{R},g}^{(r)} = \nabla_{\mathrm{R},g}^{(r)}\boldsymbol{\Theta}_g^{(r)\mathsf{H}} = \nabla_{\mathrm{E},g}^{(r)}\boldsymbol{\Theta}_g^{(r)\mathsf{H}} - \boldsymbol{\Theta}_g^{(r)}\nabla_{\mathrm{E},g}^{(r)\mathsf{H}}. \qquad (34)$$

After gradient translation, the deviation parameter and conjugate direction can be determined similarly to (28) and (27)

$$\tilde{\gamma}_g^{(r)} = \frac{\mathrm{tr}\big((\tilde{\nabla}_{\mathrm{R},g}^{(r)} - \tilde{\nabla}_{\mathrm{R},g}^{(r-1)})\tilde{\nabla}_{\mathrm{R},g}^{(r)\mathsf{H}}\big)}{\mathrm{tr}\big(\tilde{\nabla}_{\mathrm{R},g}^{(r-1)}\tilde{\nabla}_{\mathrm{R},g}^{(r-1)\mathsf{H}}\big)}. \qquad (35)$$

$$\mathbf{D}_g^{(r)} = \tilde{\nabla}_{\mathrm{R},g}^{(r)} + \tilde{\gamma}_g^{(r)}\mathbf{D}_g^{(r-1)}, \qquad (36)$$

The solution can thus be updated along the geodesic in a multiplicative rotational manner

$$\boldsymbol{\Theta}_g^{(r+1)} = \mathbf{G}_g^{(r)}(\mu) = \exp(\mu\mathbf{D}_g^{(r)})\boldsymbol{\Theta}_g^{(r)}, \qquad (37)$$

where an appropriate μ may be obtained by the Armijo rule. To double the step size, one can simply square the rotation matrix instead of recomputing the matrix exponential, that is, $\exp^2(\mu\mathbf{D}_g^{(r)}) = \exp(2\mu\mathbf{D}_g^{(r)})$. We highlight that the proposed geodesic RCG method has been tailored to the Stiefel manifold.

Algorithm 1 summarizes the proposed BD-RIS design framework based on group-wise geodesic RCG. Compared to the general non-geodesic approach, it leverages the Lie group properties to replace the add-then-retract update (31) with a multiplicative rotational update (37) along geodesics of the Stiefel manifold. This leads to faster convergence and simplifies the step size tuning thanks to appropriate parameter

space. Convergence to a local optimum is still guaranteed if not initialized at a stationary point. Note that the group-wise updates can be performed in parallel to facilitate large-scale BD-RIS optimization problems. Since the set of block-unitary matrices are algebraically closed under multiplication, one can also avoid group-wise updates by directly operating on $\boldsymbol{\Theta}$ and pinching (i.e., keeping the main block diagonal and nulling others) the Euclidean gradient (25), which can further accelerate the algorithm when the number of group is large.

We would like to give a quick overview of what we have done so far. [say why the analytical results are limited to what cases.] In this section, we solve channel power gain maximization problem in closed-form and then extend the discussion to achievable rate maximization problem. The implication of the former on the latter is investigated.

C. Pareto Frontier Characterization

We now characterize the Pareto frontier of singular values of a general $N_\mathrm{T} \times N_\mathrm{S} \times N_\mathrm{R}$ channel (2) by maximizing their weighted sum

$$\max_{\boldsymbol{\Theta}} \quad \sum_n \rho_n \sigma_n(\mathbf{H}) \qquad (38\mathrm{a})$$

$$\text{s.t.} \quad \boldsymbol{\Theta}_g^{\mathsf{H}}\boldsymbol{\Theta}_g = \mathbf{I}, \quad \forall g, \qquad (38\mathrm{b})$$

where $n \in [N]$ is the maximum channel rank, and ρ_n is the weight of the n-th singular value that can be positive, zero, or negative. Varying $\{\rho_n\}_{n\in[N]}$ characterizes the Pareto frontier enclosing the singular value region such that problem (38) generalizes most singular value shaping problems. It can be solved optimally by Algorithm 1 with the Euclidean gradient given in Lemma 1.

Lemma 1. *The Euclidean gradient of* (38a) *with respect to BD-RIS group g is*

$$\frac{\partial \sum_n \rho_n \sigma_n(\mathbf{H})}{\partial \boldsymbol{\Theta}_g^*} = \mathbf{H}_{\mathrm{B},g}^{\mathsf{H}}\mathbf{U}\mathrm{diag}(\rho_1,...,\rho_N)\mathbf{V}^{\mathsf{H}}\mathbf{H}_{\mathrm{F},g}^{\mathsf{H}}, \qquad (39)$$

where $\mathbf{U}$ and $\mathbf{V}$ are the left and right compact singular matrices of $\mathbf{H}$, respectively.

Proof. Please refer to Appendix G. □

We now analyze the computational complexity of solving Pareto singular value problem (38) by Algorithm 1. To update each BD-RIS group, compact SVD of $\mathbf{H}$ requires $\mathcal{O}(NN_\mathrm{T}N_\mathrm{R})$, Euclidean gradient (39) requires $\mathcal{O}(LN(N_\mathrm{T}+N_\mathrm{R}+L+1))$, Riemannian gradient translation (34) requires $\mathcal{O}(L^3)$, deviation parameter (35) and conjugate direction (36) together require $\mathcal{O}(L^2)$, and matrix exponential (37) requires $\mathcal{O}(L^3)$ operations [61]. The overall complexity is thus $\mathcal{O}(I_\mathrm{RCG}G(NN_\mathrm{T}N_\mathrm{R} + LN(N_\mathrm{T}+N_\mathrm{R}+L+1)+I_\mathrm{BLS}L^3))$, where I_RCG and I_BLS are the number of iterations for geodesic RCG and backtracking line search (i.e., line $13 - 18$ of Algorithm 1), respectively.

TABLE I
AVERAGE PERFORMANCE OF GEODESIC AND NON-GEODESIC RCG ALGORITHMS ON PROBLEM (38)

RCG path	$N_{\mathrm{S}} = 16$			$N_{\mathrm{S}} = 256$		
	Objective	Iterations	Time [s]	Objective	Iterations	Time [s]
Geodesic	4.359×10^{-3}	11.59	1.839×10^{-2}	1.163×10^{-2}	25.58	3.461
Non-geodesic	4.329×10^{-3}	30.92	5.743×10^{-2}	1.116×10^{-2}	61.40	13.50

2) Low-Complexity Solution: We finally propose a suboptimal two-stage solution to problem (46) that decouples the joint RIS-transceiver design. The idea is to first consider channel shaping and replace the rate maximization subproblem (47) by channel power gain maximization problem (40), then proceed to conventional eigenmode transmission (49). Both steps are solved in closed form and the computational complexity is $\mathcal{O}\big(I_{\mathrm{SAA}}G\big(N_{\mathrm{T}}N_{\mathrm{R}} + (G+1)(NL^2 + N_{\mathrm{T}}N_{\mathrm{R}}L) + L^3\big) + NN_{\mathrm{T}}N_{\mathrm{R}}\big)$. While suboptimal, this shaping-inspired solution avoids outer iterations and efficiently handles inner iterations.

V. SIMULATION RESULTS

In this section, we provide numerical results to evaluate the proposed BD-RIS designs.[10] Consider a distance-dependent path loss model $\Lambda(d) = \Lambda_0 d^{-\gamma}$ where Λ_0 is the reference path loss at distance $1\,\mathrm{m}$, d is the propagation distance, and γ is the path loss exponent. The small-scale fading model is $\mathbf{H} = \sqrt{\kappa/(1+\kappa)}\mathbf{H}_{\mathrm{LoS}} + \sqrt{1/(1+\kappa)}\mathbf{H}_{\mathrm{NLoS}}$, where κ is the Rician K-factor, $\mathbf{H}_{\mathrm{LoS}}$ is the deterministic LoS component, and $\mathbf{H}_{\mathrm{NLoS}} \sim \mathcal{CN}(\mathbf{0}, \mathbf{I})$ is the Rayleigh component. We set $\Lambda_0 = -30\,\mathrm{dB}$, $d_{\mathrm{D}} = 14.7\,\mathrm{m}$, $d_{\mathrm{F}} = 10\,\mathrm{m}$, $d_{\mathrm{B}} = 6.3\,\mathrm{m}$, $\gamma_{\mathrm{D}} = 3$, $\gamma_{\mathrm{F}} = 2.4$ and $\gamma_{\mathrm{B}} = 2$ for reference, which corresponds to a typical indoor environment with $\Lambda_{\mathrm{D}} = -65\,\mathrm{dB}$, $\Lambda_{\mathrm{F}} = -54\,\mathrm{dB}$, $\Lambda_{\mathrm{B}} = -46\,\mathrm{dB}$. The indirect path via RIS is thus $35\,\mathrm{dB}$ weaker than the direct path. Rayleigh fading (i.e., $\kappa = 0$) is assumed for all channels unless otherwise specified.

A. Algorithm Evaluation

We first compare in Table I the geodesic and non-geodesic RCG algorithm on problem (38) in an $N_{\mathrm{T}} = N_{\mathrm{R}} = 4$ system with BD-RIS group size $L = 4$. The statistics are averaged over 100 independent runs. It is observed that the geodesic RCG method achieves a slightly higher objective value with significantly (down to 1/3) lower number of iterations and shorter (down to 1/4) computational time than the non-geodesic method. The results demonstrate the efficiency of the proposed geodesic RCG algorithm especially for large-scale BD-RIS design problems.

B. Channel Singular Values Redistribution

1) Pareto Frontier: Fig. 2 shows the Pareto singular values of an $N_{\mathrm{T}} = N_{\mathrm{R}} = 2$ MIMO reshaped by a RIS. When the direct channel is negligible, the achievable regions in Fig. 2(a) are shaped like pizza slices. This is because $\sigma_1(\mathbf{H}) \geq \sigma_2(\mathbf{H}) \geq 0$ and there exists a trade-off between the alignment of two spaces.

[10]The simulation code is publicly available at https://github.com/snowztail/channel-shaping.
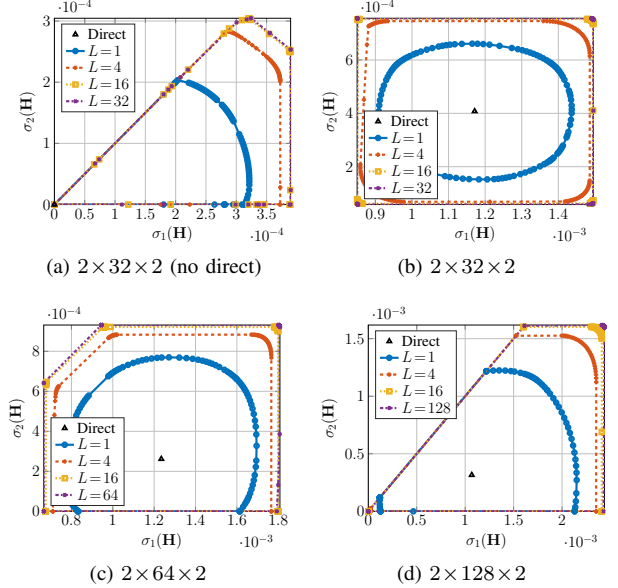
Fig. 2. Pareto frontiers of singular values of an $N_{\mathrm{T}} = N_{\mathrm{R}} = 2$ channel reshaped by BD-RIS.

We observe that the smallest singular value can be enhanced up to 2×10^{-4} by D-RIS and 3×10^{-4} by fully-connected BD-RIS, corresponding to a $50\,\%$ gain. When the direct channel is significant, the shape of the singular value region depends heavily on the relative strength of the indirect channels. In Fig. 2(b), a 32-element RIS is insufficient to compensate the $35\,\mathrm{dB}$ path loss imbalance and results in a limited singular value region that is symmetric around the direct point. As the group size L increases, the shape of the region evolves from elliptical to square. This transformation not only improves the dynamic range of $\sigma_1(\mathbf{H})$ and $\sigma_2(\mathbf{H})$ by $22\,\%$ and $38\,\%$, but also provides a better trade-off in manipulating both singular values. It suggests the design flexibility from larger group size allows better alignment of multiple singular vector spaces simultaneously. The singular value region also enlarges as the number of scattering elements N_{S} increases. In particular, Fig. 2(d) shows that the equivalent channel can be completely nulled (corresponding to the origin) by a 128-element BD-RIS thanks to its superior channel shaping capability, but not by a diagonal one. Those results demonstrate the superior channel shaping capability of BD-RIS and emphasizes the importance of reconfigurable inter-connections between elements.

2) Analytical Bounds and Numerical Results: Fig. 3 illustrates the analytical singular value bounds in Proposition 2 and the numerical results obtained by solving problem (38) with $\rho_n = \pm 1$ and $\rho_{n'} = 0$, $\forall n' \neq n$. Here we assume a rank-k

(a) $4 \times 32 \times 4$ (rank-1)

(b) $4 \times 64 \times 4$ (rank-1)

(c) $4 \times 128 \times 4$ (rank-2)

(d) $4 \times 256 \times 4$ (rank-4)

Fig. 3. Achievable channel singular values: analytical bounds (green lines) and numerical optimization results (blue and red bars). The intersections of the blue and red bars denote the singular values of the direct channel. The blue (resp. red) bars are obtained by solving problem (38) with $\rho_n = -1$ (resp. $+1$) and $\rho_{n'} = 0$, $\forall n' \neq n$. 'D' means D-RIS and 'BD' refers to fully-connected BD-RIS. 'rank-k' refers to the rank of the forward channel.

(a) $1 \times 256 \times 1$ (no direct)

(b) $4 \times 256 \times 4$ (no direct)

Fig. 4. Average maximum channel power gain versus BD-RIS group size and MIMO dimensions. The direct channel is negligible. 'Cascaded' refers to the available power of the cascaded channel, i.e., the sum of (sorted) element-wise power product of backward and forward channels.
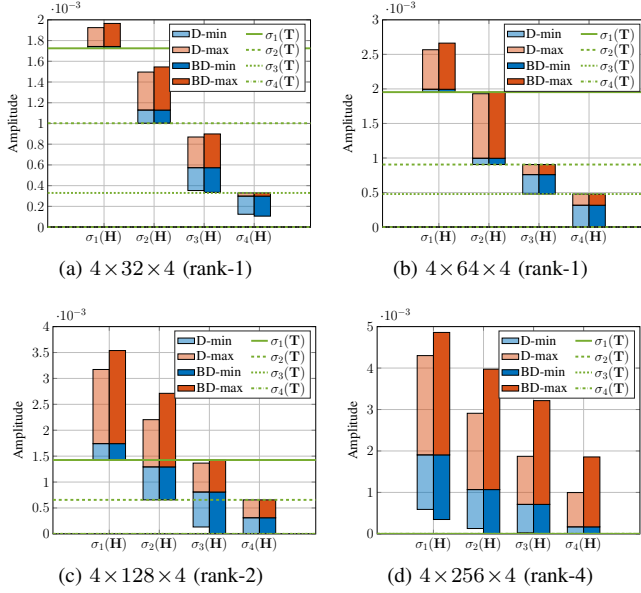

(a) $16 \times N_{\mathrm{S}} \times 16$ (no direct)

(b) $16 \times N_{\mathrm{S}} \times 16$

Fig. 5. Average maximum channel power gain versus RIS configuration. 'OP-left' and 'OP-right' refer to the suboptimal solutions to problem (40) by lossy transformation (42) where $\mathbf{\Theta}$ is to the left and right of the product, respectively.

forward channel without loss of generality. When the RIS is in the vicinity of the transmitter, Figs. 3(a) and 3(b) show that the achievable channel singular values indeed satisfy Corollary 2.1, namely $\sigma_1(\mathbf{H}) \geq \sigma_1(\mathbf{T})$, $\sigma_2(\mathbf{T}) \leq \sigma_2(\mathbf{H}) \leq \sigma_1(\mathbf{T})$, etc. It is obvious that BD-RIS can approach those bounds better than D-RIS especially for a small N_{S}. Another example is given in Fig. 3(c) with rank-2 forward channel. The first two channel singular values are unbounded above and bounded below by the first two singular values of $\mathbf{T}$, while the last two singular values can be suppressed to zero and bounded above by the first two singular values of $\mathbf{T}$. Those observations align with Proposition 2. Finally, Fig. 3(d) confirms there are no extra singular value bounds when both backward and forward channels are full-rank. This can be predicted from (9) where the compact singular matrix $\mathbf{V}_{\mathrm{F}}$ becomes unitary and $\mathbf{T} = \mathbf{0}$. The numerical results are consistent with the analytical bounds, and we conclude that the channel shaping advantage of BD-RIS over D-RIS scales with backward and forward channel ranks.

Fig. 4 compares the analytical channel power bound in Corollary 3.4 and the numerical results obtained by solving problem (40) when the direct channel is negligible. Here, a fully-connected BD-RIS can attain the upper bound either in closed form (21) or via optimization approach (44). For the SISO case in Fig. 4(a), the maximum channel power gain is approximately 4×10^{-6} by D-RIS and 6.5×10^{-6} by fully-connected BD-RIS, corresponding to a 62.5% gain. It comes purely from branch matching and agrees with the asymptotic power scaling law derived for SISO in [30, Equation 30]. Interestingly, this relative power gain surges to 270% in $N_{\mathrm{T}} = N_{\mathrm{R}} = 4$ MIMO as shown in Fig. 4(b), which can also be predicted from the expectation analysis (23). We thus conclude that the power gain of BD-RIS scales with group size and
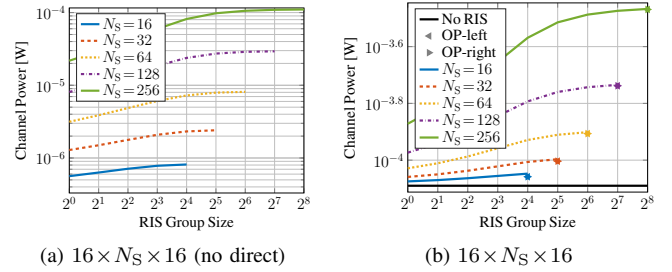
MIMO dimensions.

C. Power Gain and Achievable Rate Maximization

We first focus on channel power gain maximization problem (40). Fig. 5 shows the maximum channel power under different RIS configurations. An interesting observation is that the relative power gain of BD-RIS over D-RIS is even larger when the direct channel is significant. For example, a 64-element fully BD-RIS can almost provide the same channel power gain as a 256-element D-RIS in Fig. 5(b), but not in Fig. 5(a). This is because the RIS needs to balance the multiplicative forward-backward combining and the additive direct-indirect combining, such that the mode alignment advantage of BD-RIS becomes more pronounced. We also notice that the suboptimal solutions (43) for fully-connected BD-RIS by lossy transformation (42) are very close to optimal especially for a large N_{S}.

Fig. 6 presents the achievable rate under different MIMO and RIS configurations. At a transmit power $P = 10\,\mathrm{dB}$, Fig. 6(a) shows that introducing a 128-element D-RIS to $N_{\mathrm{T}} = N_{\mathrm{R}} = 4$ MIMO can improve the achievable rate from $22.2\,\mathrm{bps/Hz}$ to $29.2\,\mathrm{bps/Hz}$ ($+31.5\%$). A BD-RIS of group size 4 and 128 can further elevate those to $32.1\,\mathrm{bps/Hz}$ ($+44.6\%$) and $34\,\mathrm{bps/Hz}$ ($+53.2\%$), respectively. An interesting observation is that the rate gap between the optimal AO approach (47) – (49) and the shaping-inspired solution (44), (49) narrows at larger group size and completely vanishes for a fully-connected BD-RIS. This implies that joint RIS-transceiver designs can be decoupled by first shaping the wireless channel and then optimizing the active beamformer, which significantly simplifies the process at marginal performance cost. Figs. 6(b) and 6(c) also show that
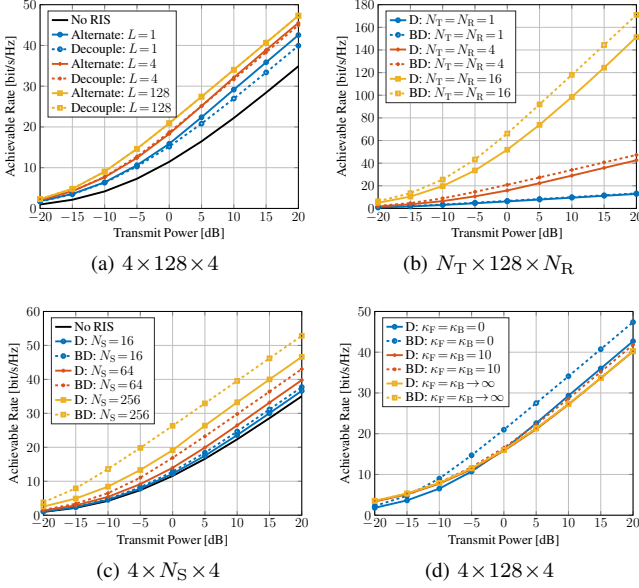
Fig. 6. Average achievable rate versus MIMO and RIS configurations. The noise power is $\eta = -75\,\text{dB}$, corresponding to a direct SNR of -10 to $30\,\text{dB}$. 'Alternate' refers to the alternating optimization and 'Decouple' refers to the low-complexity design. 'D' means D-RIS and 'BD' refers to fully-connected BD-RIS.

both *absolute and relative* rate gains of BD-RIS versus D-RIS increases with the number of transmit and receive antennas and scattering elements, especially at high SNR. For $N_S = 128$ and $P = 20\,\text{dB}$, the achievable rate ratio of BD-RIS over D-RIS is 1.04, 1.11, and 1.13 for $N_T = N_R = 1$, 4, and 16, respectively. For $N_T = N_R = 4$ and $P = 20\,\text{dB}$, this ratio amounts to 1.03, 1.08, and 1.13 for $N_S = 16$, 64, and 256, respectively. Those observations align with the power gain results in Fig. 5 and highlight the rate benefits of BD-RIS over D-RIS in large-scale MIMO systems. In the low power regime (-20 to $-10\,\text{dB}$), we also notice that the slope of the achievable rate of BD-RIS is steeper than that of D-RIS. That is, BD-RIS can help to activate more streams and achieve the asymptotic DoF at a low transmit SNR. This is particularly visible in Fig. 6(c) where the topmost curve is almost a linear function of the transmit power. It is expected from the shaping results in Fig. 2 that BD-RIS can significantly enlarge all channel singular values for higher receive SNR. Finally, Fig. 6(d) shows that the gap between D- and BD-RIS narrows as the Rician K-factor increases and becomes indistinguishable in LoS environment. The observation is expected from previous studies [30], [31], [47] and aligns with Corollary 2.1, which suggests that the BD-RIS should be deployed in rich-scattering environments to exploit its channel shaping potential.

VI. Conclusion

This paper analyzes the channel shaping capability of RIS in terms of singular values redistribution. We consider a general BD architecture that allows elements within the same group to interact, enabling more sophisticated manipulation than D-RIS. This translates to a wider dynamic range of and better tradeoff between singular values and significant power and rate gains,

especially in large-scale MIMO systems. We characterize the Pareto frontiers of channel singular values via optimization approach and provide analytical bounds for practical deployment scenarios. Specifically, the former is done by proposing an efficient RCG algorithm for BD-RIS optimization problems, which converges much faster than existing methods. We also present two beamforming designs for rate maximization problem, one for optimal performance and the other exploits channel shaping for lower complexity. Extensive simulations show that the shaping advantage of BD-RIS stems from its superior branch matching and mode alignment potentials, which scales with the number of elements, group size, and MIMO dimensions.

Appendix

A. Proof of Proposition 1

The scattering matrix of BD-RIS can be decomposed as

$$\boldsymbol{\Theta} = \mathbf{L}\boldsymbol{\Theta}_D\mathbf{R}^H, \tag{50}$$

where $\boldsymbol{\Theta}_D \in \mathbb{U}^{N_S \times N_S}$ corresponds to D-RIS and $\mathbf{L}, \mathbf{R} \in \mathbb{U}^{N_S \times N_S}$ are block-diagonal matrices of $L \times L$ unitary blocks. Manipulating $\mathbf{L}$ and $\mathbf{R}$ rotates the linear spans of $\bar{\mathbf{H}}_B \triangleq \mathbf{H}_B\mathbf{L}$ and $\bar{\mathbf{H}}_F \triangleq \mathbf{R}^H\mathbf{H}_F$ and maintains their rank. On the other hand, there exists a $\boldsymbol{\Theta}_D$ such that

$$\begin{aligned}\text{rank}(\mathbf{H}_B\boldsymbol{\Theta}_D\mathbf{H}_F) &= \min\big(\text{rank}(\mathbf{H}_B), \text{rank}(\boldsymbol{\Theta}_D), \text{rank}(\mathbf{H}_F)\big)\\ &= \min\big(\text{rank}(\bar{\mathbf{H}}_B), N_S, \text{rank}(\bar{\mathbf{H}}_F)\big)\\ &= \max_{\boldsymbol{\Theta}} \text{rank}(\mathbf{H}_B\boldsymbol{\Theta}\mathbf{H}_F)\end{aligned}$$

The same result holds if the direct channel is significant and the proof is omitted here.

B. Proof of Proposition 2

We consider rank-k forward channel and the proof follows similarly for rank-k backward channel. Let $\mathbf{H}_F = \mathbf{U}_F\boldsymbol{\Sigma}_F\mathbf{V}_F^H$ be the compact SVD of the forward channel. The channel Gram matrix $\mathbf{G} \triangleq \mathbf{H}\mathbf{H}^H$ can be written as

$$\begin{aligned}\mathbf{G} &= \mathbf{H}_D\mathbf{H}_D^H + \mathbf{H}_B\boldsymbol{\Theta}\mathbf{U}_F\boldsymbol{\Sigma}_F\boldsymbol{\Sigma}_F^H\mathbf{U}_F^H\boldsymbol{\Theta}^H\mathbf{H}_B^H\\ &\quad + \mathbf{H}_B\boldsymbol{\Theta}\mathbf{U}_F\boldsymbol{\Sigma}_F\mathbf{V}_F^H\mathbf{H}_D^H + \mathbf{H}_D\mathbf{V}_F\boldsymbol{\Sigma}_F\mathbf{U}_F^H\boldsymbol{\Theta}^H\mathbf{H}_B^H\\ &= \mathbf{H}_D(\mathbf{I} - \mathbf{V}_F\mathbf{V}_F^H)\mathbf{H}_D^H\\ &\quad + (\mathbf{H}_B\boldsymbol{\Theta}\mathbf{U}_F\boldsymbol{\Sigma}_F + \mathbf{H}_D\mathbf{V}_F)(\boldsymbol{\Sigma}_F\mathbf{U}_F^H\boldsymbol{\Theta}^H\mathbf{H}_B^H + \mathbf{V}_F^H\mathbf{H}_D^H)\\ &= \mathbf{Y} + \mathbf{Z}\mathbf{Z}^H,\end{aligned}$$

where we define $\mathbf{Y} \triangleq \mathbf{H}_D(\mathbf{I} - \mathbf{V}_F\mathbf{V}_F^H)\mathbf{H}_D^H \in \mathbb{H}^{N_R \times N_R}$ and $\mathbf{Z} \triangleq \mathbf{H}_B\boldsymbol{\Theta}\mathbf{U}_F\boldsymbol{\Sigma}_F + \mathbf{H}_D\mathbf{V}_F \in \mathbb{C}^{N_R \times k}$. That is to say, $\mathbf{G}$ can be expressed as a Hermitian matrix plus k rank-1 perturbations. According to the Cauchy interlacing formula [64, Theorem 8.4.3], the n-th eigenvalue of $\mathbf{G}$ is bounded by

$$\lambda_n(\mathbf{G}) \leq \lambda_{n-k}(\mathbf{Y}), \qquad \text{if } n > k, \tag{51}$$
$$\lambda_n(\mathbf{G}) \geq \lambda_n(\mathbf{Y}), \qquad \text{if } n < N-k+1. \tag{52}$$

Since $\mathbf{Y} = \mathbf{T}\mathbf{T}^H$ is positive semi-definite, taking the square roots of (51) and (52) gives (8a) and (8b).

C. Proof of Proposition 3

Let $\mathbf{H}_\mathrm{B} = \mathbf{U}_\mathrm{B}\boldsymbol{\Sigma}_\mathrm{B}\mathbf{V}_\mathrm{B}^\mathsf{H}$ and $\mathbf{H}_\mathrm{F} = \mathbf{U}_\mathrm{F}\boldsymbol{\Sigma}_\mathrm{F}\mathbf{V}_\mathrm{F}^\mathsf{H}$ be the SVD of the backward and forward channels, respectively. The scattering matrix of fully-connected BD-RIS can be decomposed as

$$\boldsymbol{\Theta} = \mathbf{V}_\mathrm{B}\mathbf{X}\mathbf{U}_\mathrm{F}^\mathsf{H}, \tag{53}$$

where $\mathbf{X} \in \mathbb{U}^{N_\mathrm{S} \times N_\mathrm{S}}$ is a unitary matrix to be designed. The equivalent channel is thus a function of $\mathbf{X}$

$$\mathbf{H} = \mathbf{H}_\mathrm{B}\boldsymbol{\Theta}\mathbf{H}_\mathrm{F} = \mathbf{U}_\mathrm{B}\boldsymbol{\Sigma}_\mathrm{B}\mathbf{X}\boldsymbol{\Sigma}_\mathrm{F}\mathbf{V}_\mathrm{F}^\mathsf{H}. \tag{54}$$

Since $\mathrm{sv}(\mathbf{U}\mathbf{A}\mathbf{V}^\mathsf{H}) = \mathrm{sv}(\mathbf{A})$ for unitary $\mathbf{U}$ and $\mathbf{V}$, we have

$$\begin{aligned}
\mathrm{sv}(\mathbf{H}) &= \mathrm{sv}(\mathbf{U}_\mathrm{B}\boldsymbol{\Sigma}_\mathrm{B}\mathbf{X}\boldsymbol{\Sigma}_\mathrm{F}\mathbf{V}_\mathrm{F}^\mathsf{H}) \\
&= \mathrm{sv}(\boldsymbol{\Sigma}_\mathrm{B}\mathbf{X}\boldsymbol{\Sigma}_\mathrm{F}) \\
&= \mathrm{sv}(\bar{\mathbf{U}}_\mathrm{B}\boldsymbol{\Sigma}_\mathrm{B}\bar{\mathbf{V}}_\mathrm{B}^\mathsf{H}\bar{\mathbf{U}}_\mathrm{F}\boldsymbol{\Sigma}_\mathrm{F}\bar{\mathbf{V}}_\mathrm{F}^\mathsf{H}) \\
&= \mathrm{sv}(\mathbf{B}\mathbf{F}),
\end{aligned}$$

where $\bar{\mathbf{U}}_\mathrm{B/F}$ and $\bar{\mathbf{V}}_\mathrm{B/F}$ are arbitrary unitary matrices.

D. Proof of Corollary 3.2

(13a) is one of the many inequalities enclosed in (12) when $r = k$. On the other hand, 11 implies that $\det(\mathbf{H}) = \det(\mathbf{B}\mathbf{F}) = \det(\mathbf{B})\det(\mathbf{F}) = \det(\mathbf{H}_\mathrm{B})\det(\mathbf{H}_\mathrm{F})$ and thus

$$\prod_{n=1}^{\bar{N}} \sigma_n(\mathbf{H}) = \prod_{n=1}^{\bar{N}} \sigma_n(\mathbf{H}_\mathrm{B})\sigma_n(\mathbf{H}_\mathrm{F}). \tag{55}$$

(55) together with (13a) and the non-negativity of singular values results in (13b).

E. Proof of Corollary 3.3

F. Proof of Corollary 3.4

From (53) and (54) we have

$$\begin{aligned}
\|\mathbf{H}\|_\mathrm{F}^2 &= \mathrm{tr}\big(\mathbf{V}_\mathrm{F}\boldsymbol{\Sigma}_\mathrm{F}^\mathsf{H}\mathbf{X}^\mathsf{H}\boldsymbol{\Sigma}_\mathrm{B}^\mathsf{H}\mathbf{U}_\mathrm{B}^\mathsf{H}\mathbf{U}_\mathrm{B}\boldsymbol{\Sigma}_\mathrm{B}\mathbf{X}\boldsymbol{\Sigma}_\mathrm{F}\mathbf{V}_\mathrm{F}^\mathsf{H}\big) \\
&= \mathrm{tr}\big(\boldsymbol{\Sigma}_\mathrm{B}^\mathsf{H}\boldsymbol{\Sigma}_\mathrm{B} \cdot \mathbf{X}\boldsymbol{\Sigma}_\mathrm{F}\boldsymbol{\Sigma}_\mathrm{F}^\mathsf{H}\mathbf{X}^\mathsf{H}\big) \\
&\triangleq \mathrm{tr}\big(\tilde{\mathbf{B}}\tilde{\mathbf{F}}\big),
\end{aligned} \tag{56}$$

where $\mathbf{X} \triangleq \mathbf{V}_\mathrm{B}^\mathsf{H}\boldsymbol{\Theta}\mathbf{U}_\mathrm{F} \in \mathbb{U}^{N_\mathrm{S} \times N_\mathrm{S}}$, $\tilde{\mathbf{B}} \triangleq \boldsymbol{\Sigma}_\mathrm{B}^\mathsf{H}\boldsymbol{\Sigma}_\mathrm{B} \in \mathbb{H}_+^{N_\mathrm{S} \times N_\mathrm{S}}$, and $\tilde{\mathbf{F}} \triangleq \mathbf{X}\boldsymbol{\Sigma}_\mathrm{F}\boldsymbol{\Sigma}_\mathrm{F}^\mathsf{H}\mathbf{X}^\mathsf{H} \in \mathbb{H}_+^{N_\mathrm{S} \times N_\mathrm{S}}$. By Ruhe's trace inequality for positive semi-definite matrices [68, H.1.g and H.1.h],

$$\sum_n \lambda_n(\tilde{\mathbf{B}})\lambda_{N_\mathrm{S}-n+1}(\tilde{\mathbf{F}}) \le \mathrm{tr}(\tilde{\mathbf{B}}\tilde{\mathbf{F}}) \le \sum_n \lambda_n(\tilde{\mathbf{B}})\lambda_n(\tilde{\mathbf{F}}),$$

which simplifies to (19). The upper bound is attained when $\mathbf{X}$ is chosen to match the singular values of $\tilde{\mathbf{F}}$ to those of $\tilde{\mathbf{B}}$ in similar order. Apparently this occurs at $\mathbf{X} = \mathbf{I}$ and $\boldsymbol{\Theta} = \mathbf{V}_\mathrm{B}\mathbf{U}_\mathrm{F}^\mathsf{H}$. On the other hand, the lower bound is attained when the singular values of $\tilde{\mathbf{F}}$ and $\tilde{\mathbf{B}}$ are matched in reverse order, namely $\mathbf{X} = \mathbf{J}$ and $\boldsymbol{\Theta} = \mathbf{V}_\mathrm{B}\mathbf{J}\mathbf{U}_\mathrm{F}^\mathsf{H}$.

G. Proof of Lemma 1

Let $\mathbf{H} = \sum_n \mathbf{u}_n\sigma_n\mathbf{v}_n^\mathsf{H}$ be the compact SVD of the equivalent channel. Since the singular vectors are orthonormal, the n-th singular value can be expressed as

$$\sigma_n = \mathbf{u}_n^\mathsf{H}\mathbf{H}\mathbf{v}_n = \mathbf{u}_n^\mathsf{T}\mathbf{H}^*\mathbf{v}_n^*, \tag{57}$$

whose differential with respect to $\boldsymbol{\Theta}_g^*$ is

$$\begin{aligned}
\partial\sigma_n &= \partial\mathbf{u}_n^\mathsf{T}\underbrace{\mathbf{H}^*\mathbf{v}_n^*}_{\sum_m \mathbf{u}_m^*\sigma_m\mathbf{v}_m^\mathsf{T}\mathbf{v}_n} + \mathbf{u}_n^\mathsf{T}\cdot\partial\mathbf{H}^*\cdot\mathbf{v}_n^* + \underbrace{\mathbf{u}_n^\mathsf{T}\mathbf{H}^*}_{\mathbf{u}_n^\mathsf{T}\sum_m \mathbf{u}_m^*\sigma_m\mathbf{v}_m^\mathsf{T}}\partial\mathbf{v}_n^* \\
&= \underbrace{\partial\mathbf{u}_n^\mathsf{T}\mathbf{u}_n^*}_{\partial 1 = 0}\sigma_n + \mathbf{u}_n^\mathsf{T}\cdot\partial\mathbf{H}^*\cdot\mathbf{v}_n^* + \sigma_n\cdot\underbrace{\mathbf{v}_n^\mathsf{T}\partial\mathbf{v}_n^*}_{\partial 1 = 0} \\
&= \mathbf{u}_n^\mathsf{T}\mathbf{H}_{\mathrm{B},g}^*\cdot\partial\boldsymbol{\Theta}_g^*\cdot\mathbf{H}_{\mathrm{F},g}^*\mathbf{v}_n^* \\
&= \mathrm{tr}(\mathbf{H}_{\mathrm{F},g}^*\mathbf{v}_n^*\mathbf{u}_n^\mathsf{T}\mathbf{H}_{\mathrm{B},g}^*\cdot\partial\boldsymbol{\Theta}_g^*).
\end{aligned}$$

According to [69], the corresponding complex derivative is

$$\frac{\partial\sigma_n}{\partial\boldsymbol{\Theta}_g^*} = \mathbf{H}_{\mathrm{B},g}^\mathsf{H}\mathbf{u}_n\mathbf{v}_n^\mathsf{H}\mathbf{H}_{\mathrm{F},g}^\mathsf{H}. \tag{58}$$

A linear combination of (58) yields (39).

H. Proof of Proposition 4

The differential of (40a) with respect to $\boldsymbol{\Theta}_g^*$ is

$$\begin{aligned}
\partial\|\mathbf{H}\|_\mathrm{F}^2 &= \mathrm{tr}\big(\mathbf{H}_{\mathrm{B},g}^*\cdot\partial\boldsymbol{\Theta}_g^*\cdot\mathbf{H}_{\mathrm{F},g}^*(\mathbf{H}_\mathrm{D}^\mathsf{T} + \mathbf{H}_\mathrm{F}^\mathsf{T}\boldsymbol{\Theta}^\mathsf{T}\mathbf{H}_\mathrm{B}^\mathsf{T})\big) \\
&= \mathrm{tr}\big(\mathbf{H}_{\mathrm{F},g}^*(\mathbf{H}_\mathrm{D}^\mathsf{T} + \mathbf{H}_\mathrm{F}^\mathsf{T}\boldsymbol{\Theta}^\mathsf{T}\mathbf{H}_\mathrm{B}^\mathsf{T})\mathbf{H}_{\mathrm{B},g}^*\cdot\partial\boldsymbol{\Theta}_g^*\big)
\end{aligned}$$

and the corresponding complex derivative is

$$\frac{\partial\|\mathbf{H}\|_\mathrm{F}^2}{\partial\boldsymbol{\Theta}_g^*} = \mathbf{H}_{\mathrm{B},g}^\mathsf{H}(\mathbf{H}_\mathrm{D} + \mathbf{H}_\mathrm{B}\boldsymbol{\Theta}\mathbf{H}_\mathrm{F})\mathbf{H}_{\mathrm{F},g}^\mathsf{H} = \mathbf{M}_g. \tag{59}$$

First, we approximate the quadratic objective (40a) by its local Taylor expansion

$$\max_{\boldsymbol{\Theta}} \quad \sum_g 2\Re\big\{\mathrm{tr}(\boldsymbol{\Theta}_g^\mathsf{H}\mathbf{M}_g)\big\} \tag{60a}$$

$$\text{s.t.} \quad \boldsymbol{\Theta}_g^\mathsf{H}\boldsymbol{\Theta}_g = \mathbf{I}, \quad \forall g. \tag{60b}$$

Let $\mathbf{M}_g = \mathbf{U}_g\boldsymbol{\Sigma}_g\mathbf{V}_g^\mathsf{H}$ be the compact SVD of $\mathbf{M}_g$. We have

$$\Re\big\{\mathrm{tr}(\boldsymbol{\Theta}_g^\mathsf{H}\mathbf{M}_g)\big\} = \Re\big\{\mathrm{tr}(\boldsymbol{\Sigma}_g\mathbf{V}_g^\mathsf{H}\boldsymbol{\Theta}_g^\mathsf{H}\mathbf{U}_g)\big\} \le \mathrm{tr}(\boldsymbol{\Sigma}_g). \tag{61}$$

The upper bound is tight when $\mathbf{V}_g^\mathsf{H}\boldsymbol{\Theta}_g^\mathsf{H}\mathbf{U}_g = \mathbf{I}$, which implies the optimal solution of (60) is $\tilde{\boldsymbol{\Theta}}_g = \mathbf{U}_g\mathbf{V}_g^\mathsf{H}$, $\forall g$.

Next, we prove that solving (60) successively does not decrease (40a). Since $\tilde{\boldsymbol{\Theta}}$ optimal for problem (60), we have $\sum_g 2\Re\big\{\mathrm{tr}(\tilde{\boldsymbol{\Theta}}_g^\mathsf{H}\mathbf{M}_g)\big\} \ge \sum_g 2\Re\big\{\mathrm{tr}(\boldsymbol{\Theta}_g^\mathsf{H}\mathbf{M}_g)\big\}$ which is explicitly expressed by (63). On the other hand, expanding $\|\sum_g \mathbf{H}_{\mathrm{B},g}\tilde{\boldsymbol{\Theta}}_g\mathbf{H}_{\mathrm{F},g} - \sum_g \mathbf{H}_{\mathrm{B},g}\boldsymbol{\Theta}_g\mathbf{H}_{\mathrm{F},g}\|_\mathrm{F}^2 \ge 0$ gives (64). Adding (63) and (64), we have

$$\begin{aligned}
& 2\Re\big\{\mathrm{tr}(\tilde{\boldsymbol{\Theta}}^\mathsf{H}\mathbf{H}_\mathrm{B}^\mathsf{H}\mathbf{H}_\mathrm{D}\mathbf{H}_\mathrm{F}^\mathsf{H})\big\} + \mathrm{tr}(\mathbf{H}_\mathrm{F}^\mathsf{H}\tilde{\boldsymbol{\Theta}}^\mathsf{H}\mathbf{H}_\mathrm{B}^\mathsf{H}\mathbf{H}_\mathrm{B}\tilde{\boldsymbol{\Theta}}\mathbf{H}_\mathrm{F}) \\
& \ge 2\Re\big\{\mathrm{tr}(\boldsymbol{\Theta}^\mathsf{H}\mathbf{H}_\mathrm{B}^\mathsf{H}\mathbf{H}_\mathrm{D}\mathbf{H}_\mathrm{F}^\mathsf{H})\big\} + \mathrm{tr}(\mathbf{H}_\mathrm{F}^\mathsf{H}\boldsymbol{\Theta}^\mathsf{H}\mathbf{H}_\mathrm{B}^\mathsf{H}\mathbf{H}_\mathrm{B}\boldsymbol{\Theta}\mathbf{H}_\mathrm{F}),
\end{aligned} \tag{62}$$

which suggests that updating $\tilde{\boldsymbol{\Theta}}$ does not decrease (40a).

Finally, we prove that the converging point of (60), denoted by $\tilde{\boldsymbol{\Theta}}^?$, is a stationary point of (40). The Karush-Kuhn-Tucker (KKT) conditions of (40) and (60) are equivalent in terms of

$$2\Re\left\{\sum_g \mathrm{tr}(\tilde{\boldsymbol{\Theta}}_g^{\mathsf{H}}\mathbf{H}_{\mathrm{B},g}^{\mathsf{H}}\mathbf{H}_{\mathrm{D}}\mathbf{H}_{\mathrm{F},g}^{\mathsf{H}}) + \sum_{g_1,g_2}\mathrm{tr}(\tilde{\boldsymbol{\Theta}}_{g_1}^{\mathsf{H}}\mathbf{H}_{\mathrm{B},g_1}^{\mathsf{H}}\mathbf{H}_{\mathrm{B},g_2}\boldsymbol{\Theta}_{g_2}\mathbf{H}_{\mathrm{F},g_2}\mathbf{H}_{\mathrm{F},g_1}^{\mathsf{H}})\right\} \geq 2\Re\left\{\sum_g \mathrm{tr}(\boldsymbol{\Theta}_g^{\mathsf{H}}\mathbf{H}_{\mathrm{B},g}^{\mathsf{H}}\mathbf{H}_{\mathrm{D}}\mathbf{H}_{\mathrm{F},g}^{\mathsf{H}}) + \sum_{g_1,g_2}\mathrm{tr}(\boldsymbol{\Theta}_{g_1}^{\mathsf{H}}\mathbf{H}_{\mathrm{B},g_1}^{\mathsf{H}}\mathbf{H}_{\mathrm{B},g_2}\boldsymbol{\Theta}_{g_2}\mathbf{H}_{\mathrm{F},g_2}\mathbf{H}_{\mathrm{F},g_1}^{\mathsf{H}})\right\} \quad (63)$$

$$\sum_{g_1,g_2}\mathrm{tr}(\mathbf{H}_{\mathrm{F},g_1}^{\mathsf{H}}\tilde{\boldsymbol{\Theta}}_{g_1}^{\mathsf{H}}\mathbf{H}_{\mathrm{B},g_1}^{\mathsf{H}}\mathbf{H}_{\mathrm{B},g_2}\tilde{\boldsymbol{\Theta}}_{g_2}\mathbf{H}_{\mathrm{F},g_2}) - 2\Re\left\{\sum_{g_1,g_2}\mathrm{tr}(\mathbf{H}_{\mathrm{F},g_1}^{\mathsf{H}}\tilde{\boldsymbol{\Theta}}_{g_1}^{\mathsf{H}}\mathbf{H}_{\mathrm{B},g_1}^{\mathsf{H}}\mathbf{H}_{\mathrm{B},g_2}\boldsymbol{\Theta}_{g_2}\mathbf{H}_{\mathrm{F},g_2})\right\} + \sum_{g_1,g_2}\mathrm{tr}(\mathbf{H}_{\mathrm{F},g_1}^{\mathsf{H}}\boldsymbol{\Theta}_{g_1}^{\mathsf{H}}\mathbf{H}_{\mathrm{B},g_1}^{\mathsf{H}}\mathbf{H}_{\mathrm{B},g_2}\boldsymbol{\Theta}_{g_2}\mathbf{H}_{\mathrm{F},g_2}) \geq 0 \quad (64)$$

---

primal/dual feasibility and complementary slackness, while the stationary conditions are respectively, $\forall g$,

$$\mathbf{H}_{\mathrm{B},g}^{\mathsf{H}}(\mathbf{H}_{\mathrm{D}} + \mathbf{H}_{\mathrm{B}}\boldsymbol{\Theta}^{\star}\mathbf{H}_{\mathrm{F}})\mathbf{H}_{\mathrm{F},g}^{\mathsf{H}} - \boldsymbol{\Theta}_g^{\star}\boldsymbol{\Lambda}_g^{\mathsf{H}} = 0, \quad (65)$$

$$\mathbf{M}_g - \boldsymbol{\Theta}_g^{\star}\boldsymbol{\Lambda}_g^{\mathsf{H}} = 0. \quad (66)$$

On convergence, (66) becomes $\mathbf{H}_{\mathrm{B},g}^{\mathsf{H}}(\mathbf{H}_{\mathrm{D}} + \mathbf{H}_{\mathrm{B}}\boldsymbol{\Theta}^{?}\mathbf{H}_{\mathrm{F}})\mathbf{H}_{\mathrm{F},g}^{\mathsf{H}} - \boldsymbol{\Theta}_g^{?}\boldsymbol{\Lambda}_g^{\mathsf{H}} = 0$ and reduces to (65). The proof is thus completed.

I. Proof of Lemma 2

The differential of R with respect to $\boldsymbol{\Theta}_g^*$ is [69]

$$\begin{aligned}\partial R &= \frac{1}{\eta}\mathrm{tr}\left\{\partial\mathbf{H}^* \cdot \mathbf{Q}^{\mathsf{T}}\mathbf{H}^{\mathsf{T}}\left(\mathbf{I} + \frac{\mathbf{H}^*\mathbf{Q}^{\mathsf{T}}\mathbf{H}^{\mathsf{T}}}{\eta}\right)^{-1}\right\}\\&= \frac{1}{\eta}\mathrm{tr}\left\{\mathbf{H}_{\mathrm{B},g}^* \cdot \partial\boldsymbol{\Theta}_g^* \cdot \mathbf{H}_{\mathrm{F},g}^*\mathbf{Q}^{\mathsf{T}}\mathbf{H}^{\mathsf{T}}\left(\mathbf{I} + \frac{\mathbf{H}^*\mathbf{Q}^{\mathsf{T}}\mathbf{H}^{\mathsf{T}}}{\eta}\right)^{-1}\right\}\\&= \frac{1}{\eta}\mathrm{tr}\left\{\mathbf{H}_{\mathrm{F},g}^*\mathbf{Q}^{\mathsf{T}}\mathbf{H}^{\mathsf{T}}\left(\mathbf{I} + \frac{\mathbf{H}^*\mathbf{Q}^{\mathsf{T}}\mathbf{H}^{\mathsf{T}}}{\eta}\right)^{-1}\mathbf{H}_{\mathrm{B},g}^* \cdot \partial\boldsymbol{\Theta}_g^*\right\},\end{aligned}$$

and the corresponding complex derivative is (48).

REFERENCES

[1] E. Basar, M. D. Renzo, J. D. Rosny, M. Debbah, M.-S. Alouini, and R. Zhang, "Wireless communications through reconfigurable intelligent surfaces," *IEEE Access*, vol. 7, pp. 116 753–116 773, 2019.

[2] Q. Wu and R. Zhang, "Intelligent reflecting surface enhanced wireless network via joint active and passive beamforming," *IEEE Transactions on Wireless Communications*, vol. 18, pp. 5394–5409, Nov 2019.

[3] H. Guo, Y.-C. Liang, J. Chen, and E. G. Larsson, "Weighted sum-rate maximization for reconfigurable intelligent surface aided wireless networks," *IEEE Transactions on Wireless Communications*, vol. 19, pp. 3064–3076, May 2020.

[4] Y. Liu, Y. Zhang, X. Zhao, S. Geng, P. Qin, and Z. Zhou, "Dynamic-controlled RIS assisted multi-user MISO downlink system: Joint beamforming design," *IEEE Transactions on Green Communications and Networking*, vol. 6, pp. 1069–1081, Jun 2022.

[5] Y. He, Y. Cai, H. Mao, and G. Yu, "RIS-assisted communication radar coexistence: Joint beamforming design and analysis," *IEEE Journal on Selected Areas in Communications*, vol. 40, pp. 2131–2145, Jul 2022.

[6] H. Luo, R. Liu, M. Li, Y. Liu, and Q. Liu, "Joint beamforming design for RIS-assisted integrated sensing and communication systems," *IEEE Transactions on Vehicular Technology*, vol. 71, pp. 13 393–13 397, Dec 2022.

[7] M. Hua, Q. Wu, C. He, S. Ma, and W. Chen, "Joint active and passive beamforming design for IRS-aided radar-communication," *IEEE Transactions on Wireless Communications*, vol. 22, pp. 2278–2294, Apr 2023.

[8] Q. Wu and R. Zhang, "Joint active and passive beamforming optimization for intelligent reflecting surface assisted SWIPT under QoS constraints," *IEEE Journal on Selected Areas in Communications*, vol. 38, no. 8, pp. 1735–1748, Aug 2020.

[9] Z. Feng, B. Clerckx, and Y. Zhao, "Waveform and beamforming design for intelligent reflecting surface aided wireless power transfer: Single-user and multi-user solutions," *IEEE Transactions on Wireless Communications*, 2022.

[10] Y. Zhao, B. Clerckx, and Z. Feng, "IRS-aided SWIPT: Joint waveform, active and passive beamforming design under nonlinear harvester model," *IEEE Transactions on Communications*, vol. 70, pp. 1345–1359, 2022.

[11] R. Karasik, O. Simeone, M. D. Renzo, and S. S. Shitz, "Beyond max-SNR: Joint encoding for reconfigurable intelligent surfaces," in *2020 IEEE International Symposium on Information Theory (ISIT)*, Jun 2020, pp. 2965–2970.

[12] E. Basar, "Reconfigurable intelligent surface-based index modulation: A new beyond MIMO paradigm for 6G," *IEEE Transactions on Communications*, vol. 68, pp. 3187–3196, May 2020.

[13] J. Ye, S. Guo, S. Dang, B. Shihada, and M.-S. Alouini, "On the capacity of reconfigurable intelligent surface assisted MIMO symbiotic communications," *IEEE Transactions on Wireless Communications*, vol. 21, pp. 1943–1959, Mar 2022.

[14] Y.-C. Liang, Q. Zhang, E. G. Larsson, and G. Y. Li, "Symbiotic radio: Cognitive backscattering communications for future wireless networks," *IEEE Transactions on Cognitive Communications and Networking*, vol. 6, pp. 1242–1255, Dec 2020.

[15] Y. Zhao and B. Clerckx, "RIScatter: Unifying backscatter communication and reconfigurable intelligent surface," *IEEE Journal on Selected Areas in Communications*, pp. 1–1, Dec 2024.

[16] H. Yang, H. Ding, K. Cao, M. Elkashlan, H. Li, and K. Xin, "A RIS-segmented symbiotic ambient backscatter communication system," *IEEE Transactions on Vehicular Technology*, vol. 73, pp. 812–825, Jan 2024.

[17] E. Basar, "Reconfigurable intelligent surfaces for doppler effect and multipath fading mitigation," *Frontiers in Communications and Networks*, vol. 2, May 2021.

[18] E. Arslan, I. Yildirim, F. Kilinc, and E. Basar, "Over-the-air equalization with reconfigurable intelligent surfaces," *IET Communications*, vol. 16, pp. 1486–1497, Aug 2022.

[19] O. Ozdogan, E. Bjornson, and E. G. Larsson, "Using intelligent reflecting surfaces for rank improvement in MIMO communications," in *ICASSP 2020 - 2020 IEEE International Conference on Acoustics, Speech and Signal Processing (ICASSP)*, May 2020, pp. 9160–9164.

[20] Y. Yang, B. Zheng, S. Zhang, and R. Zhang, "Intelligent reflecting surface meets OFDM: Protocol design and rate maximization," *IEEE Transactions on Communications*, vol. 68, pp. 4522–4535, Jul 2020.

[21] G. Chen and Q. Wu, "Fundamental limits of intelligent reflecting surface aided multiuser broadcast channel," *IEEE Transactions on Communications*, vol. 71, pp. 5904–5919, Oct 2023.

[22] M. A. ElMossallamy, H. Zhang, R. Sultan, K. G. Seddik, L. Song, G. Y. Li, and Z. Han, "On spatial multiplexing using reconfigurable intelligent surfaces," *IEEE Wireless Communications Letters*, vol. 10, pp. 226–230, Feb 2021.

[23] S. Meng, W. Tang, W. Chen, J. Lan, Q. Y. Zhou, Y. Han, X. Li, and S. Jin, "Rank optimization for MIMO channel with RIS: Simulation and measurement," *IEEE Wireless Communications Letters*, vol. 13, pp. 437–441, Feb 2024.

[24] Y. Zheng, T. Lin, and Y. Zhu, "Passive beamforming for IRS-assisted MU-MIMO systems with one-bit ADCs: An SER minimization design approach," *IEEE Communications Letters*, vol. 26, pp. 1101–1105, May 2022.

[25] W. Huang, B. Lei, S. He, C. Kai, and C. Li, "Condition number improvement of IRS-aided near-field MIMO channels," in *2023 IEEE International Conference on Communications Workshops (ICC Workshops)*, May 2023, pp. 1210–1215.

[26] A. H. Bafghi, V. Jamali, M. Nasiri-Kenari, and R. Schober, "Degrees of freedom of the K-user interference channel assisted by active and passive IRSs," *IEEE Transactions on Communications*, vol. 70, pp. 3063–3080, May 2022.

[27] S. Zheng, B. Lv, T. Zhang, Y. Xu, G. Chen, R. Wang, and P. C. Ching, "On DoF of active RIS-assisted MIMO interference channel with arbitrary antenna configurations: When will RIS help?" *IEEE Transactions on Vehicular Technology*, Dec 2023.

[28] S. H. Chae and K. Lee, "Cooperative communication for the rank-deficient MIMO interference channel with a reconfigurable intelligent surface," *IEEE Transactions on Wireless Communications*, vol. 22, pp. 2099–2112, Mar 2023.

[29] S. Shen and B. Clerckx, "Beamforming optimization for MIMO wireless power transfer with nonlinear energy harvesting: RF combining versus DC combining," *IEEE Transactions on Wireless Communications*, vol. 20, pp. 199–213, Jan 2021.

[30] S. Shen, B. Clerckx, and R. Murch, "Modeling and architecture design of reconfigurable intelligent surfaces using scattering parameter network

analysis," *IEEE Transactions on Wireless Communications*, vol. 21, pp. 1229–1243, Feb 2022.

[31] M. Nerini, S. Shen, and B. Clerckx, "Closed-form global optimization of beyond diagonal reconfigurable intelligent surfaces," *IEEE Transactions on Wireless Communications*, vol. 23, pp. 1037–1051, Feb 2024.

[32] M. Nerini, S. Shen, H. Li, and B. Clerckx, "Beyond diagonal reconfigurable intelligent surfaces utilizing graph theory: Modeling, architecture design, and optimization," *IEEE Transactions on Wireless Communications*, pp. 1–1, May 2024.

[33] I. Santamaria, M. Soleymani, E. Jorswieck, and J. Gutiérrez, "SNR maximization in beyond diagonal RIS-assisted single and multiple antenna links," *IEEE Signal Processing Letters*, vol. 30, pp. 923–926, 2023.

[34] ——, "Interference leakage minimization in RIS-assisted MIMO interference channels," in *ICASSP 2023 - 2023 IEEE International Conference on Acoustics, Speech and Signal Processing (ICASSP)*, vol. 39, Jun 2023, pp. 1–5.

[35] H.-R. Ahn, *Asymmetric Passive Components in Microwave Integrated Circuits*. Hoboken, NJ, USA: Wiley, 2006.

[36] H. Li, S. Shen, and B. Clerckx, "Beyond diagonal reconfigurable intelligent surfaces: A multi-sector mode enabling highly directional full-space wireless coverage," *IEEE Journal on Selected Areas in Communications*, vol. 41, pp. 2446–2460, Aug 2023.

[37] H. Li, S. Shen, Y. Zhang, and B. Clerckx, "Channel estimation and beamforming for beyond diagonal reconfigurable intelligent surfaces," *arXiv:2403.18087*, 2024.

[38] H. Li, S. Shen, M. Nerini, M. D. Renzo, and B. Clerckx, "Beyond diagonal reconfigurable intelligent surfaces with mutual coupling: Modeling and optimization," *IEEE Communications Letters*, pp. 1–1, Oct 2024.

[39] H. Li, M. Nerini, S. Shen, and B. Clerckx, "Wideband modeling and beamforming for beyond diagonal reconfigurable intelligent surfaces," *arXiv:2403.12893*, 2024.

[40] T. Fang and Y. Mao, "A low-complexity beamforming design for beyond-diagonal RIS aided multi-user networks," *IEEE Communications Letters*, pp. 1–1, Jul 2023.

[41] Y. Zhou, Y. Liu, H. Li, Q. Wu, S. Shen, and B. Clerckx, "Optimizing power consumption, energy efficiency and sum-rate using beyond diagonal RIS — a unified approach," *IEEE Transactions on Wireless Communications*, pp. 1–1, 2023.

[42] M. Soleymani, I. Santamaria, E. Jorswieck, and B. Clerckx, "Optimization of rate-splitting multiple access in beyond diagonal RIS-assisted URLLC systems," *IEEE Transactions on Wireless Communications*, pp. 1–1, Jul 2024.

[43] G. Bartoli, A. Abrardo, N. Decarli, D. Dardari, and M. D. Renzo, "Spatial multiplexing in near field MIMO channels with reconfigurable intelligent surfaces," *IET Signal Processing*, vol. 17, Mar 2023.

[44] A. Mishra, Y. Mao, C. D'Andrea, S. Buzzi, and B. Clerckx, "Transmitter side beyond-diagonal reconfigurable intelligent surface for massive MIMO networks," *IEEE Wireless Communications Letters*, vol. 13, pp. 352–356, Feb 2024.

[45] M. Nerini, S. Shen, and B. Clerckx, "Discrete-value group and fully connected architectures for beyond diagonal reconfigurable intelligent surfaces," *IEEE Transactions on Vehicular Technology*, vol. 72, pp. 16 354–16 368, Dec 2023.

[46] M. T. Ivrlac and J. A. Nossek, "Toward a circuit theory of communication," *IEEE Transactions on Circuits and Systems I: Regular Papers*, vol. 57, pp. 1663–1683, Jul 2010.

[47] H. Li, S. Shen, and B. Clerckx, "Beyond diagonal reconfigurable intelligent surfaces: From transmitting and reflecting modes to single-, group-, and fully-connected architectures," *IEEE Transactions on Wireless Communications*, vol. 22, pp. 2311–2324, Apr 2023.

[48] D. Semmler, M. Joham, and W. Utschick, "High SNR analysis of RIS-aided MIMO broadcast channels," in *2023 IEEE 24th International Workshop on Signal Processing Advances in Wireless Communications (SPAWC)*, Sep 2023, pp. 221–225.

[49] L. Hogben, Ed., *Handbook of Linear Algebra*. Boca Raton, FL, USA: CRC press, 2013.

[50] R. A. Horn and C. R. Johnson, *Topics in Matrix Analysis*. Cambridge, UK: Cambridge University Press, Jun 1994.

[51] W. Fulton, "Eigenvalues, invariant factors, highest weights, and schubert calculus," *Bulletin of the American Mathematical Society*, vol. 37, pp. 209–249, Apr 2000.

[52] R. Bhatia, "Linear algebra to quantum cohomology: The story of alfred horn's inequalities," *The American Mathematical Monthly*, vol. 108, pp. 289–318, Apr 2001.

[53] Y. Fang, K. A. Loparo, and X. Feng, "Inequalities for the trace of matrix product," *IEEE Transactions on Automatic Control*, vol. 39, pp. 2489–2490, Dec 1994.

[54] A. Zanella, M. Chiani, and M. Win, "On the marginal distribution of the eigenvalues of wishart matrices," *IEEE Transactions on Communications*, vol. 57, pp. 1050–1060, Apr 2009.

[55] P.-A. Absil, R. Mahony, and R. Sepulchre, *Optimization Algorithms on Matrix Manifolds*. Princeton, NJ, USA: Princeton University Press, 2009.

[56] C. Pan, G. Zhou, K. Zhi, S. Hong, T. Wu, Y. Pan, H. Ren, M. D. Renzo, A. L. Swindlehurst, R. Zhang, and A. Y. Zhang, "An overview of signal processing techniques for RIS/IRS-aided wireless systems," *IEEE Journal of Selected Topics in Signal Processing*, vol. 16, pp. 883–917, Aug 2022.

[57] J. Nocedal and S. J. Wright, *Numerical Optimization*. Springer, Sep 2006.

[58] L. Armijo, "Minimization of functions having lipschitz continuous first partial derivatives," *Pacific Journal of Mathematics*, vol. 16, pp. 1–3, Jan 1966.

[59] A. Edelman, T. A. Arias, and S. T. Smith, "The geometry of algorithms with orthogonality constraints," *SIAM Journal on Matrix Analysis and Applications*, vol. 20, pp. 303–353, Jan 1998.

[60] T. E. Abrudan, J. Eriksson, and V. Koivunen, "Steepest descent algorithms for optimization under unitary matrix constraint," *IEEE Transactions on Signal Processing*, vol. 56, pp. 1134–1147, Mar 2008.

[61] C. Moler and C. V. Loan, "Nineteen dubious ways to compute the exponential of a matrix, twenty-five years later," *SIAM Review*, vol. 45, pp. 3–49, Jan 2003.

[62] J. C. Gower and G. B. Dijksterhuis, *Procrustes Problems*. Oxford, UK: Oxford University Press, 2004.

[63] T. Bell, "Global positioning system-based attitude determination and the orthogonal procrustes problem," *Journal of Guidance, Control, and Dynamics*, vol. 26, pp. 820–822, Sep 2003.

[64] G. H. Golub and C. F. V. Loan, *Matrix Computations*. Baltimore, MD, USA: Johns Hopkins University Press, 2013.

[65] F. Nie, R. Zhang, and X. Li, "A generalized power iteration method for solving quadratic problem on the Stiefel manifold," *Science China Information Sciences*, vol. 60, p. 112101, Nov 2017.

[66] B. Clerckx and C. Oestges, *MIMO Wireless Networks: Channels, Techniques and Standards for Multi-Antenna, Multi-User and Multi-Cell Systems*. Waltham, MA, USA: Academic Press, 2013.

[67] D. Tse and P. Viswanath, *Fundamentals of Wireless Communication*. Cambridge, UK: Cambridge University Press, May 2005.

[68] A. W. Marshall, I. Olkin, and B. C. Arnold, *Inequalities: Theory of Majorization and Its Applications*, 2nd ed., ser. Springer Series in Statistics. New York, NY, USA: Springer, Dec 2010.

[69] A. Hjorungnes and D. Gesbert, "Complex-valued matrix differentiation: Techniques and key results," *IEEE Transactions on Signal Processing*, vol. 55, pp. 2740–2746, Jun 2007.